

Review

Experimental Determination, Modeling, and Simulation of Nonlinear Thermal Effects in Bipolar Transistors under Static Conditions: A Critical Review and Update

Vincenzo d'Alessandro ^{1,*} , Antonio Pio Catalano ¹ , Ciro Scognamillo ¹ , Markus Müller ², Michael Schröter ², Peter J. Zampardi ³  and Lorenzo Codecasa ⁴ 

¹ Department of Electrical Engineering and Information Technology, University Federico II, 80125 Naples, Italy; antoniopio.catalano@unina.it (A.P.C.); ciro.scognamillo@unina.it (C.S.)

² Chair for Electron Devices and Integrated Circuits, Technical University Dresden, 01069 Dresden, Germany; markus.mueller3@tu-dresden.de (M.M.); mschroter@ieee.org (M.S.)

³ Qorvo, Inc., Newbury Park, CA 91320, USA; peter.zampardi@qorvo.com

⁴ Department of Electronics, Information, and Bioengineering, Politecnico di Milano, 20133 Milan, Italy; lorenzo.codecasa@polimi.it

* Correspondence: vindales@unina.it

Abstract: This paper presents a comprehensive overview of nonlinear thermal effects in bipolar transistors under static conditions. The influence of these effects on the thermal resistance is theoretically explained and analytically modeled using the single-semiconductor assumption. A detailed review of experimental techniques to extract the thermal resistance as a function of backside temperature and/or dissipated power from DC measurements is provided; advantages, underlying approximations, and limitations of all methods are clarified, and guidelines for their correct application are given. Accurate FEM thermal simulations of an InGaP/GaAs and a Si/SiGe HBT are performed to verify the accuracy of the single-semiconductor theory. The thermal resistance formulations employed in the most popular compact bipolar transistor models for circuit simulators are investigated, and it is found that they do not properly describe nonlinear thermal effects. Alternative implementations of the more accurate single-semiconductor theory are then proposed for the future versions of the compact models.

Keywords: compact transistor model; finite-element method (FEM); gallium arsenide (GaAs); heterojunction bipolar transistor (HBT); nonlinear thermal effects; silicon-germanium (SiGe); thermal resistance



Citation: d'Alessandro, V.; Catalano, A.P.; Scognamillo, C.; Müller, M.; Schröter, M.; Zampardi, P.J.; Codecasa, L. Experimental Determination, Modeling, and Simulation of Nonlinear Thermal Effects in Bipolar Transistors under Static Conditions: A Critical Review and Update. *Energies* **2022**, *15*, 5457. <https://doi.org/10.3390/en15155457>

Academic Editor: Philippe Leclère

Received: 14 June 2022

Accepted: 25 July 2022

Published: 28 July 2022

Publisher's Note: MDPI stays neutral with regard to jurisdictional claims in published maps and institutional affiliations.



Copyright: © 2022 by the authors. Licensee MDPI, Basel, Switzerland. This article is an open access article distributed under the terms and conditions of the Creative Commons Attribution (CC BY) license (<https://creativecommons.org/licenses/by/4.0/>).

1. Introduction

Electrothermal (ET) effects are an important issue in modern high-frequency bipolar transistors in any technology, as they adversely impact the device behavior in multiple ways, namely, distortion in the I–V curves, which shifts the DC bias and shrinks the safe operating area [1–4], degradation of the low-frequency behavior [5], and even irreversible failure, likely to occur in multifinger devices due to thermally-induced current hogging [6,7].

Gallium arsenide (GaAs)-based heterojunction bipolar transistors (HBTs) like InGaP/GaAs and AlGaAs/GaAs, commonly considered the dominant technology for handset power amplifier design, are also plagued by strong ET effects due to the high operating power densities and high thermal resistances, the latter induced by (i) the low thermal conductivity of the GaAs substrate (one third of that of silicon), (ii) the lateral heat confinement due to mesa isolation, and (iii) the choice of interlevel dielectric films [4,6,8], ref. [9] and references therein, [10].

In silicon/silicon-germanium (Si/SiGe) HBTs for mm-wave and near-THz applications (wireless and optical communication, medical equipment, and automotive radars), ET effects are aggravated by the technology strategies employed to boost the frequency

performance, i.e., (i) adoption of shallow and deep trenches filled with oxide or polysilicon coated with oxide, which suffer from low thermal conductivity and hamper the lateral propagation of the heat emerging from the power dissipation region; horizontal scaling (ii) of the emitter, which drives higher current (and power) density, and (iii) of the spacing between the intrinsic transistor and the surrounding trenches, which further inhibits the lateral heat flow. All these factors concur to increase the thermal resistances of single-finger transistors, which have been pushed into the thousands of K/W and beyond [11–17].

As the *static* thermal behavior of any device is well represented by its thermal resistance, accurately extracting this parameter from easy-to-perform measurements and describing it with simple formulations for compact transistor models is of utmost importance for many applications, e.g., simulation of the impact of ET effects on circuit performance, determination of optimum values of ballast resistors, and reliability estimations.

Unfortunately, the extraction and modeling tasks are complicated by the *nonlinear nature* of the heat conduction problem arising from the reduction of thermal conductivity of materials with increasing temperature (*nonlinear thermal effects*), which make the thermal resistance a monotonically growing function of the backside temperature and dissipated power. Effort has been dedicated to partially/fully account for such effects (i) in techniques for the experimental extraction of the thermal resistance, and (ii) in thermal resistance formulations conceived for compact transistor models. However, detailed discussions on advantages and limitations of the extraction techniques, as well as on the accuracy of the formulations, are still missing in literature.

This paper is intended to offer an extensive and critical overview of nonlinear thermal effects in modern high-frequency bipolar transistors from a multi-fold point of view. In Section 2, the separate impact on the thermal resistance of the backside temperature and dissipated power is theoretically explained and analytically described by resorting to the simple assumption of a single-semiconductor device. In Section 3, a detailed review of the available experimental techniques to extract the thermal resistance as a function of backside temperature and/or dissipated power is offered. In particular, the analysis focuses on *indirect* methods based on straightforward and cheap measurements of voltages/currents under DC conditions. The techniques are presented in a tutorial style with a unified nomenclature; advantages, limitations, and approximations are clarified, and simple guidelines for their correct application are provided. In Section 4, 3-D nonlinear thermal simulations of an InGaP/GaAs and a Si/SiGe HBT, chosen as case studies, are performed to obtain a reliable dependence of the thermal resistance as a function of backside temperature and dissipated power for both technologies. The resulting R_{TH} data are used to verify the accuracy of the single-semiconductor theory. In Section 5, the thermal resistance formulations embedded in compact transistor models available in circuit simulators are examined. It is observed that nonlinear thermal effects are either not considered or improperly accounted for, which affects the ET simulation results for medium/high temperatures. To tackle this issue, more accurate, yet numerically efficient and stable (not prone to convergence problems) implementations of the single-semiconductor theory are proposed for the future releases of compact transistor models. Conclusions are finally given in Section 6.

2. Thermal Resistance Dependence on Nonlinear Thermal Effects

The static thermal behavior of an electron device is effectively described by the self-heating thermal resistance R_{TH} [K/W], which represents an indicator of the *inability* of the component to remove heat from the power dissipation region (heat source). By specifically referring to a bipolar transistor, R_{TH} is defined as

$$R_{TH} = \frac{T_j - T_B}{P_D} = \frac{\Delta T_j}{P_D} \quad (1)$$

where T_j is the temperature averaged over the base-emitter junction [K] (also called *junction temperature*), T_B is the backside (or baseplate, or ambient) temperature [K] that can be assigned through a thermochuck/heater, and P_D [W] is the dissipated power, given by

$$P_D = I_B \cdot V_{BE} + I_C \cdot V_{CE} = I_E \cdot V_{BE} + I_C \cdot V_{CB} \quad (2)$$

In (2), all terms have their customary meaning, namely, I_B , I_C , I_E are the base, collector, and emitter currents, respectively, while V_{BE} , V_{CE} , V_{CB} are the externally applied base-emitter, collector-emitter, and collector-base voltages, respectively. The thermal resistance is also referred to as (i) junction temperature rise above T_B normalized to P_D or (ii) static thermal response to power dissipation.

R_{TH} depends on (i) device and heat source geometry, (ii) thermal conductivities of the materials crossed by the heat emerging from the source, and (iii) boundary conditions. A transistor with a horizontally- and/or vertically-scaled heat source suffers from a higher R_{TH} (e.g., [13,18,19]), as for the same P_D the dissipated power density is higher, and therefore T_j is higher. In a similar fashion, the adoption of materials with low thermal conductivities hinders the heat flow, thus leading to an increase in R_{TH} .

Additionally, it must be considered that the thermal conductivities k [W/μmK] of semiconductors and metals in a transistor decrease with temperature, thereby lowering the heat transfer efficiency. The thermally induced k degradation introduces a *nonlinearity* in the heat conduction equation, and the resulting effects are referred to as *nonlinear thermal effects*. It is well known that in a practically relevant temperature range the k of many semiconductors of interest reduces with a power law

$$k(T) = k(T_0) \cdot \left(\frac{T}{T_0} \right)^{-\alpha} \quad (3)$$

where the reference temperature T_0 is equal to 300 K and $\alpha > 0$, while for the metals the decrease is well described by the following linear model:

$$k(T) = k(T_0) - \beta \cdot (T - T_0) \quad (4)$$

where $\beta > 0$. Commonly accepted values for $k(T_0)$, α , β corresponding to the most relevant semiconductors and metals are reported in Table 1.

Table 1. Quoted values of parameters in (3), (4) for the most important semiconductors and metals in electron devices.

Material	$k(T_0)$ [W/ μmK]	α	β [K^{-1}]
Si	1.422×10^{-4} [20] 1.45×10^{-4} [21] $1.48\text{--}1.54 \times 10^{-4}$ [22] and references therein 1.56×10^{-4} [23]	1.25 [24] 1.3 [25], also reported in [26] 1.33 from elaboration of data in [20], and [27] from elaboration of data in [21] 1.4 [28] from elaboration of data in [23] 1.65 [22], although 1.3 seems better (see Ref. [2] in [29])	-
GaAs	0.44×10^{-4} [21] $0.37\text{--}0.46 \times 10^{-4}$ [22] and references therein 0.55×10^{-4} [30]	1.25 [22] and references therein 1.27 [28] from elaboration of data in [30]	-
GaN	$1.25\text{--}1.5 \times 10^{-4}$ [22] and references therein	0.43 [22] and references therein	-
InP	0.68×10^{-4} [22] and references therein, [31] 0.696×10^{-4} [32]	1.4 [22] and references therein 1.48 [31], also reported in [28]	-
4H-SiC	3.7×10^{-4} [33,34]	1.29 [35]	-
6H-SiC	$3.2\text{--}4.9 \times 10^{-4}$ [22] and references therein 3.87×10^{-4} for the conductivity normal to the c axis; a value 30% lower for the conductivity parallel to the c axis [36] 4.9×10^{-4} [33,34,37]	1.29 [35] 1.49 for the conductivity normal to the c axis [36]	-
Al	2.39×10^{-4} from elaboration of data in [38]	-	2.1×10^{-8} from elaboration of data in [38]
Cu	3.97×10^{-4} from elaboration of data in [38]	-	5.2×10^{-8} from elaboration of data in [38]

The device temperature increases—and the thermal conductivities decrease—for *two distinct physical mechanisms*: (i) the raise in backside temperature T_B (*nonlinear thermal effect due to the backside temperature*) and (ii) the increase in dissipated power P_D (*nonlinear self-heating effect*). Consequently, R_{TH} is a monotonically growing function of both T_B and P_D and should be more properly formulated as $R_{TH}(T_B, P_D)$, which inherently accounts for nonlinear thermal effects. This means that the observed dependence on T_B and P_D does *not* come from the *explicit* presence of these quantities on the RHS of (1), which is the basic definition of thermal resistance, but *implicitly* comes from the k reduction with increasing temperature [28].

Hereafter, R_{TH00} will conventionally denote the thermal resistance of the bipolar transistor at $T_B = T_0$ and very low P_D (ideally for $P_D \rightarrow 0$ W, i.e., in the absence of the nonlinear self-heating effect), that is,

$$R_{TH00} = R_{TH}(T_B = T_0, P_D \rightarrow 0) \quad (5)$$

In simple terms, R_{TH00} represents the thermal resistance of the transistor if the thermal conductivities of all materials are equal to their $k(T_0)$ value.

The following analysis is aimed at providing an illustrative overview of the R_{TH} dependence on T_B and P_D . Let us consider an *ideal* device homogeneously composed of a specific semiconductor, the thermal conductivity of which obeys (3) (*single-semiconductor assumption*), and let us first assume that the backside temperature T_B is equal to T_0 . The typical approach used to include the impact of the nonlinear self-heating effect on the junction temperature T_j (and on R_{TH}) is the Kirchhoff transformation [39–41]. Let us define T_{j00} as the junction temperature given by

$$T_{j00} = T_0 + R_{TH00} \cdot P_D \quad (6)$$

where P_D is assumed to be very low. In this case, the temperature T_{j0P} ($>T_{j00}$) accounting for the nonlinear effect due to P_D can be calculated as [24,27,42–44]

$$T_{j0P} = T_0 \cdot \left[1 - (\alpha - 1) \cdot \frac{T_{j00} - T_0}{T_0} \right]^{\frac{-1}{\alpha-1}} = T_0 \cdot \left[1 - (\alpha - 1) \cdot \frac{R_{TH00} \cdot P_D}{T_0} \right]^{\frac{-1}{\alpha-1}} \quad (7)$$

It must be remarked that (7) also holds in the more general case of a multilayered structure where the thermal conductivities $k(T_0)$ of the layers are different but share the same power dependence on temperature (3), that is, the same value for the power factor α [26]. The thermal resistance is obtained as

$$R_{TH0P} = R_{TH}(T_B = T_0, P_D) = \frac{T_{j0P} - T_0}{P_D} = \frac{T_0}{P_D} \cdot \left\{ \left[1 - (\alpha - 1) \cdot \frac{R_{TH00} \cdot P_D}{T_0} \right]^{\frac{-1}{\alpha-1}} - 1 \right\} \quad (8)$$

and is obviously higher than the $T_B = T_0$ zero-power thermal resistance R_{TH00} .

Now let us consider an arbitrary backside temperature $T_B \geq T_0$. The R_{TH} increase due to nonlinear thermal effects *concurrently* induced by T_B and P_D can be described as follows. Since for this ideal single-semiconductor device the thermal resistance is inversely proportional to the thermal conductivity [13,17–19,28,29,39,45,46], then the R_{TH} growth only due to $T_B > T_0$ (for $P_D \rightarrow 0$ W, i.e., without the nonlinear self-heating effect) can be described by the power law [17,28,29,45]

$$R_{THB0} = R_{TH}(T_B, P_D \rightarrow 0) = R_{TH00} \cdot \left(\frac{T_B}{T_0} \right)^\alpha \quad (9)$$

It is noteworthy that also for *real* devices R_{THB0} is higher than R_{TH00} since, as mentioned before, the thermal conductivities of semiconductors and metals at T_B are lower than the reference values at T_0 . Let us designate as T_{jB0} the junction temperature given by

$$T_{jB0} = T_B + R_{THB0} \cdot P_D \quad (10)$$

for very low P_D . The Kirchhoff transformation can again be used to account for the nonlinear self-heating effect [17,28,29,43,45]

$$T_j = T_B \cdot \left[1 - (\alpha - 1) \cdot \frac{T_{jB0} - T_B}{T_B} \right]^{\frac{-1}{\alpha-1}} = T_B \cdot \left[1 - (\alpha - 1) \cdot \frac{R_{THB0} \cdot P_D}{T_B} \right]^{\frac{-1}{\alpha-1}} \quad (11)$$

and the thermal resistance can be calculated as

$$R_{TH}(T_B, P_D) = \frac{T_j - T_B}{P_D} = \frac{T_B}{P_D} \cdot \left\{ \left[1 - (\alpha - 1) \cdot \frac{R_{THB0} \cdot P_D}{T_B} \right]^{\frac{-1}{\alpha-1}} - 1 \right\} \quad (12)$$

which can also be written as

$$R_{TH}(T_B, P_D) = \frac{T_B}{P_D} \cdot \left\{ \left[1 - (\alpha - 1) \cdot \frac{R_{TH00} \cdot P_D}{T_B \cdot \left(\frac{T_0}{T_B} \right)^\alpha} \right]^{\frac{-1}{\alpha-1}} - 1 \right\} \quad (13)$$

where use has been made of (9).

As an illustrative example, we evaluated the R_{TH} behavior as a function of T_B and P_D with (13) assuming that the device is homogeneously composed of GaAs ($\alpha = 1.25$), and that its $T_B = T_0$ zero-power thermal resistance R_{TH00} is equal to 1000 K/W. Figure 1 shows $R_{TH}(T_B, P_D)$ vs. P_D and vs. T_j at different T_B values. It is important to note that, by keeping T_j constant while increasing T_B (which can be obtained by reducing P_D), R_{TH} increases. This contrasts with the common—and wrong—belief that R_{TH} only depends on T_j , and can be easily explained by considering that, for higher T_B values, all materials encountered by the heat flowing through the device will suffer from a higher temperature (falling in the range T_B to T_j), and thus from a lower thermal conductivity. Hence, accounting for nonlinear thermal effects with an R_{TH} that only depends on T_j in a compact bipolar transistor model is an unfortunate choice, as the underlying physics of the problem is incorrectly represented.

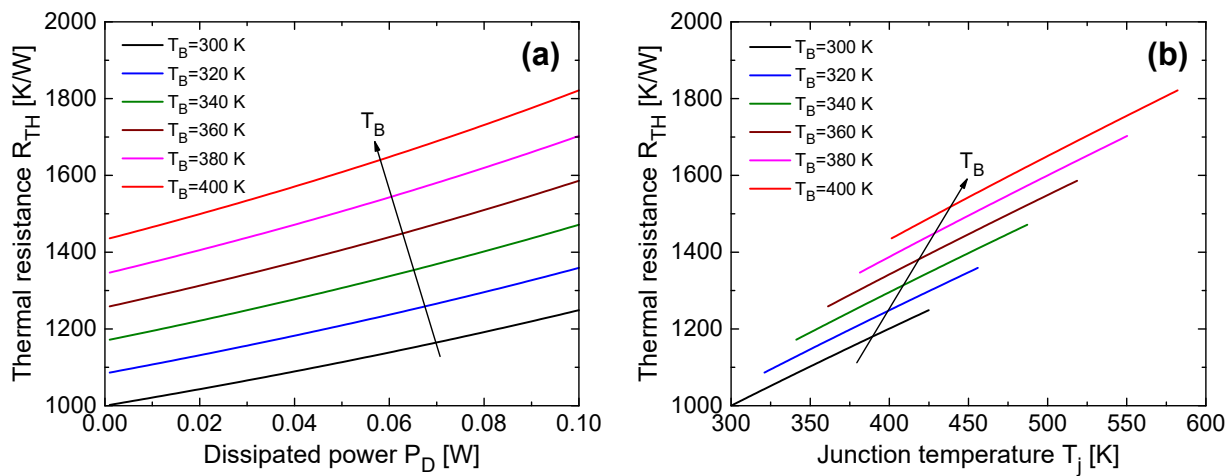


Figure 1. Thermal resistance R_{TH} as a function of (a) dissipated power P_D and (b) junction temperature T_j at $T_B = 300, 320, 340, 360, 380, 400$ K.

Starting from the single-semiconductor theory, Walkey et al. [28], and subsequently Huszka et al. [17], resort to mathematical approximations to get an $R_{TH}(T_B, P_D)$ formulation simpler than (13). First, the power law (3) is linearized as

$$k(T_B) \approx \frac{k(T_0)}{1 + \frac{\alpha}{T_0} \cdot (T_B - T_0)} \quad (14)$$

whence the zero-power thermal resistance at T_B can be expressed as

$$R_{THB0} \approx R_{TH00} \cdot \left[1 + \frac{\alpha}{T_0} \cdot (T_B - T_0) \right] = R_{TH00} \cdot [1 + \zeta_B \cdot (T_B - T_0)] \quad (15)$$

which shows a linear increase of R_{THB0} with T_B , also assumed in [47]. The $R_{TH}(T_B, P_D)$ formulation given by (12), which also includes the nonlinear self-heating effect, is then expanded in a Taylor series that retains only the first two terms, thus leading to

$$R_{TH}(T_B, P_D) \approx R_{THB0} \cdot \left(1 + \alpha \cdot \frac{R_{THB0}}{2 \cdot T_B} \cdot P_D \right) = R_{THB0} \cdot [1 + \zeta_P(T_B) \cdot P_D] \quad (16)$$

By substituting (15) into (16),

$$R_{TH}(T_B, P_D) = R_{TH00} \cdot [1 + \zeta_B \cdot (T_B - T_0)] \cdot [1 + \zeta_P(T_B) \cdot P_D] \quad (17)$$

where the α -sensitive parameters ζ_B and $\zeta_P(T_B)$ account for the separate dependence on T_B and P_D , respectively. A linear dependence of R_{TH0P} on P_D was also proposed in [2,48].

Walkey et al. also suggest a fast procedure to determine ζ_B and $\zeta_P(T_B)$ from a few experimentally extracted R_{TH} values. In particular, ζ_B can be evaluated from the zero-power thermal resistances R_{TH00} and $R_{THB10} = R_{TH}(T_{B1}, P_D \rightarrow 0)$ as

$$\zeta_B = \frac{1}{T_{B1} - T_0} \cdot \left(\frac{R_{THB10}}{R_{TH00}} - 1 \right) \quad (18)$$

while $\zeta_P(T_B)$ can be calculated for each T_B from two thermal resistances $R_{TH}(T_B, P_{D1})$ and $R_{TH}(T_B, P_{D2})$ as

$$\zeta_P(T_B) = \frac{\frac{R_{TH}(T_B, P_{D2})}{R_{TH}(T_B, P_{D1})} - 1}{P_{D2} - \frac{R_{TH}(T_B, P_{D2})}{R_{TH}(T_B, P_{D1})} \cdot P_{D1}} \quad (19)$$

3. Review of Experimental R_{TH} Extraction Techniques Accounting for Nonlinear Thermal Effects

The literature is populated by many techniques for extracting the thermal resistance of bipolar transistors from simple DC measurements (a complete review being given in [49]), which can be subdivided into (i) approaches using the relation between an easily-measurable electrical parameter (like V_{BE}) and T_j as a *thermometer*, and (ii) approaches that do not use the thermometer (e.g., those based on intersection points). This section aims to provide a systematic and comprehensive overview of the methods *explicitly* accounting for the influence of nonlinear thermal effects, namely, those determining the R_{TH} dependence on T_B (for $T_B \geq T_0$) and/or P_D , or on T_j . The techniques are explained in detail in chronological order using a unified nomenclature; advantages/drawbacks are clarified for each of them, and guidelines for their correct use are provided.

3.1. Bovolon et al.

The technique proposed by Bovolon et al. [50] is “differential” and can be considered as an extension of the approach published by Dawson et al. [51].

Let us focus on the “internal” (junction) base-emitter voltage V_{BEj} , given by

$$V_{BEj} = V_{BE} - R_B \cdot I_B - R_E \cdot I_E = V_{BE} - \frac{R_B}{\beta_F} \cdot I_C - R_E \cdot I_E \approx V_{BE} - \left(\frac{R_B}{\beta_F} + R_E \right) \cdot I_C = V_{BE} - R_{EB} \cdot I_C \quad (20)$$

where R_B and R_E are the parasitic base and emitter series resistances, respectively, and β_F is the common-emitter current gain. From simple theoretical considerations, it can be demonstrated that in the absence of Early, high-injection (Kirk), and avalanche effects, under forward mode V_{BEj} decreases almost linearly with the junction temperature T_j at a given $I_C \approx I_E$ [13]

$$V_{BEj}(T_j) = V_{BEj}(T_0) - \phi \cdot (T_j - T_0) \quad (21)$$

By making use of (20), in the assumption of a temperature-insensitive R_{EB} , (21) becomes

$$V_{BE}(T_j) = R_{EB} \cdot I_C + V_{BEj}(T_0) - \phi \cdot (T_j - T_0) = V_{BE}(T_0) - \phi \cdot (T_j - T_0) \quad (22)$$

which states that the linear behavior also holds for the externally applied V_{BE} . From (22), it is clear that the linear behavior also takes place *locally*, i.e., around a certain junction temperature T_j^* :

$$V_{BE}(T_j) = V_{BE}(T_j^*) - \phi \cdot (T_j - T_j^*) \quad (23)$$

Exploiting the definition of thermal resistance (1), (23) turns into

$$V_{BE}(T_B, P_D) = V_{BE}(T_j^*) - \phi \cdot [T_B + R_{TH}(T_B, P_D) \cdot P_D - T_j^*] \quad (24)$$

If (24) is applied to another backside temperature $T_B + \Delta T_B$ at the same dissipated power P_D ,

$$V_{BE}(T_B + \Delta T_B, P_D) = V_{BE}(T_{j*}) - \phi \cdot [T_B + \Delta T_B + R_{TH}(T_B + \Delta T_B, P_D) \cdot P_D - T_{j*}] \quad (25)$$

By subtracting (25) from (24),

$$V_{BE}(T_B, P_D) - V_{BE}(T_B + \Delta T_B, P_D) = \phi \cdot \Delta T_B + \phi \cdot [R_{TH}(T_B + \Delta T_B, P_D) - R_{TH}(T_B, P_D)] \cdot P_D \quad (26)$$

If ΔT_B is chosen sufficiently low, (26) reduces to

$$V_{BE}(T_B, P_D) - V_{BE}(T_B + \Delta T_B, P_D) \approx \phi \cdot \Delta T_B \quad (27)$$

from which coefficient ϕ describing the temperature dependence of V_{BE} (the thermometer) can be determined as

$$\phi = \frac{V_{BE}(T_B, P_D) - V_{BE}(T_B + \Delta T_B, P_D)}{\Delta T_B} \quad (28)$$

Subsequently, by applying (24) to another dissipated power $P_D + \Delta P_D$ at the same backside temperature T_B ,

$$V_{BE}(T_B, P_D + \Delta P_D) = V_{BE}(T_{j*}) - \phi \cdot [T_B + R_{TH}(T_B, P_D + \Delta P_D) \cdot (P_D + \Delta P_D) - T_{j*}] \quad (29)$$

By subtracting (29) from (24),

$$V_{BE}(T_B, P_D) - V_{BE}(T_B, P_D + \Delta P_D) = \phi \cdot [R_{TH}(T_B, P_D + \Delta P_D) \cdot (P_D + \Delta P_D) - R_{TH}(T_B, P_D) \cdot P_D] \quad (30)$$

If ΔP_D is chosen sufficiently small, (30) reduces to

$$V_{BE}(T_B, P_D) - V_{BE}(T_B, P_D + \Delta P_D) \approx \phi \cdot R_{TH}(T_B, P_D) \cdot \Delta P_D \quad (31)$$

and finally, combining (31) and (28),

$$R_{TH}(T_B, P_D) = \frac{V_{BE}(T_B, P_D) - V_{BE}(T_B, P_D + \Delta P_D)}{\phi \cdot \Delta P_D} = \frac{\frac{V_{BE}(T_B, P_D) - V_{BE}(T_B, P_D + \Delta P_D)}{\Delta P_D}}{\frac{V_{BE}(T_B, P_D) - V_{BE}(T_B + \Delta T_B, P_D)}{\Delta T_B}} \quad (32)$$

By repeating the extraction for different values of backside temperature T_B and dissipated power P_D , R_{TH} can be determined as a function of T_B and P_D without imposing analytical assumptions on both dependences.

For each (T_B, P_D) couple, the approach requires the measurement of two I_B -constant I_C - V_{CE} characteristics and of the corresponding V_{BE} - V_{CE} curves at T_B and $T_B + \Delta T_B$. On the first I_C - V_{CE} characteristic, two points with close dissipated powers P_D and $P_D + \Delta P_D$ are selected, and the related $V_{BE}(T_B, P_D)$, $V_{BE}(T_B, P_D + \Delta P_D)$ values are used for the calculation of the numerator of (32). Then, the point with dissipated power P_D has to be identified on the second characteristic, and the associated $V_{BE}(T_B + \Delta T_B, P_D)$ allows the calculation of the denominator of (32); if this point has not been exactly measured, an interpolation between the adjacent points is required.

The technique must be cautiously applied for multiple reasons: (i) ΔT_B should be chosen sufficiently small to ensure (27); (ii) ΔP_D should be chosen sufficiently low to lead to (31); (iii) moreover, the collector currents corresponding to P_D and $P_D + \Delta P_D$ should be quite similar, as coefficient ϕ is dependent on I_C [1,3,6,8,11,13,52,53]; (iv) finally, it must be remarked that both the ϕ (28) and R_{TH} (32) calculations are determined by a difference between V_{BE} values measured in *two* points only, which can in principle jeopardize the accuracy of the results. Due to all the above aspects, the practical application of the technique can be judged as nontrivial.

3.2. Yeats

The technique conceived by Yeats [45] can also be reviewed as an improved version of that presented by Dawson et al. [51]. First, some V_{BE} – V_{CE} (V_{CE} being given by the sum of the forced V_{CB} and the measured V_{BE}) characteristics are measured at a given I_E and various backside temperatures T_B . Through a quadratic polynomial, the V_{BE} values corresponding to $V_{CE} = 0$ V ($P_D = 0$ W and thus $T_j = T_B$) are extrapolated, so that the V_{BE} – T_j thermometer is defined at the assigned I_E and then inverted (turned into T_j – V_{BE}) and described by means of a quadratic polynomial with I_E -dependent coefficients. Hence, any V_{BE} is associated to the corresponding T_j value, and the experimental I_E -constant T_j – P_D curves at various T_B are straightforwardly determined. Consequently, the experimental $R_{TH}(T_B, P_D)$ against P_D is known for each T_B from (1) without imposing assumptions on these dependences. This technique is often applied to GaAs-based HBTs, especially for T_j estimates used in reliability.

Yeats proposes to adopt the single-semiconductor theory shown in Section 2 to analytically describe the measured $R_{TH}(T_B, P_D)$ data; hence, he uses (13), where (9) models the influence of T_B , and the Kirchhoff transformation is adopted to include the sensitivity to P_D . An optimization routine (referred to as “brute-force 2-D search”) is exploited, which allows achieving R_{TH00} and α that favor the best aggregate match between all the experimental R_{TH} data and (13). Here Yeats remarks that, as the correlated parameters R_{TH00} and α are simultaneously optimized, R_{TH00} might differ from the extracted $T_B = T_0$ zero-power thermal resistance, although the calibrated (R_{TH00}, α) couple well describes the measured data; conveniently, the numerical analysis reported in Section 4 shows that the optimized R_{TH00} is very close to the simulated value over wide T_B and P_D ranges, regardless of the HBT technology.

Although the technique seems to be simple and effective, there are two questionable aspects to point out: the first is the extrapolation procedure needed to calibrate the V_{BE} – T_j thermometer, the accuracy of which should be further investigated, and the second is the *direct* use of the thermometer to find the T_j , and thus the $R_{TH}(T_B, P_D)$, associated to a specific V_{BE} , which makes the R_{TH} results too sensitive to the precision of the V_{BE} measurements (other thermometer-based techniques do not *directly* use the thermometer to evaluate R_{TH} , but, like Bovolon et al. [50], exploit another step requiring the “differential” calculation $\Delta V_{BE} / \Delta P_D$ or even the derivative dV_{BE} / dP_D ; this alleviates the impact of inaccuracies on the V_{BE} measurements).

3.3. Marsh

In contrast to [45,50], which require a calibrated thermometer, the technique conceived by Marsh [47] belongs to a category of indirect approaches (the word “direct” in the title could mislead) based on intersections between curves, and allows a relatively simple extraction of R_{THB0} as a function of T_B . Marsh proposes to measure three I_C – V_{CE} characteristics by forcing the same I_B at three backside temperatures $T_{B1} < T_{B2} < T_{B3}$. In HBTs, a negative-differential-resistance (NDR) region arises (I_C reduces with V_{CE}) under forward mode due to the negative temperature coefficient (NTC) of the current gain β_F , in turn induced by the wider bandgap of the emitter compared to that of the base. In the NDR, three points can be identified, which correspond to the same I_C , but are associated to different V_{CE} ($V_{CE1} > V_{CE2} > V_{CE3}$), and thus different dissipated powers P_D ($P_{D1} > P_{D2} > P_{D3}$). As I_C and I_B are the same at these points, β_F is the same, and, since β_F only depends on T_j , T_j is also the same. Consequently, using (1), the following equations hold in the points:

$$\begin{aligned} T_j &= T_{B1} + R_{TH}(T_{B1}, P_{D1}) \cdot P_{D1} \\ T_j &= T_{B2} + R_{TH}(T_{B2}, P_{D2}) \cdot P_{D2} \\ T_j &= T_{B3} + R_{TH}(T_{B3}, P_{D3}) \cdot P_{D3} \end{aligned} \quad (33)$$

Marsh assumes that R_{TH} is a linearly increasing function of T_B , while neglecting its P_D dependence, that is,

$$R_{TH}(T_B, P_D) \approx R_{THB0} = A_{Marsh} + B_{Marsh} \cdot T_B \quad (34)$$

By substituting (34) into (33), a three-equation system with three unknowns (A_{Marsh} , B_{Marsh} , T_j) is obtained

$$\begin{aligned} T_j &= T_{B1} + (A_{Marsh} + B_{Marsh} \cdot T_{B1}) \cdot P_{D1} \\ T_j &= T_{B2} + (A_{Marsh} + B_{Marsh} \cdot T_{B2}) \cdot P_{D2} \\ T_j &= T_{B3} + (A_{Marsh} + B_{Marsh} \cdot T_{B3}) \cdot P_{D3} \end{aligned} \quad (35)$$

from which it is possible to determine the junction temperature T_j at the selected points, as well as R_{TH} as a function of T_B as given by (34). Such a linear relation can also be written as

$$R_{THB0} = A_{Marsh} + B_{Marsh} \cdot T_0 + B_{Marsh} \cdot (T_B - T_0) = R_{TH00} + B_{Marsh} \cdot (T_B - T_0) \quad (36)$$

It is worth noting that in principle this technique can also be applied to Si bipolar junction transistors (BJTs), which show a positive-differential-resistance (PDR) behavior in the I_B -constant I_C - V_{CE} curves due to the positive temperature coefficient (PTC) of β_F , in turn induced by the narrower bandgap of the highly-doped emitter compared to that of the base; however, in this case the R_{TH} extraction would be affected by the Early effect, which is not accounted for in the approach and can be misinterpreted as an additional self-heating.

From the numerical investigation reported in Section 4, it will be found that the R_{THB0} vs. T_B behavior is almost linear in the T_B span 300 to 450 K. However, attention must be paid during the practical application of this technique, as P_{D1} , P_{D2} , P_{D3} must be chosen sufficiently low to prevent a significant nonlinear self-heating effect.

3.4. Paasschens et al.

Paasschens and his co-authors [29] invoke the single-semiconductor theory shown in Section 2, and, like [17,28,45], consider (9) for the dependence of the zero-power thermal resistance R_{THB0} on T_B , and the Kirchhoff-based (13) for the complete $R_{TH}(T_B, P_D)$ formulation. The authors only perform low-power measurements of R_{THB0} at various T_B values with the technique proposed in [54], which can be categorized as a “differential” approach not based on a thermometer. Once the thermal resistance R_{TH00} is extracted, parameter α is optimized by comparison between (9) and experimental data, and then also used in (13). In other words, Paasschens et al. do not measure the impact of the nonlinear self-heating effect on R_{TH} , which is instead done in [45,50].

The technique presented in [54] can be summarized as follows. The transistor is in a common-emitter configuration with the backside at temperature T_B , and the forced V_{BE} and V_{CE} are chosen to keep P_D low.

Let us derive the R_{TH} expression used in the procedure. The collector current I_C is a function of the independent variables V_{BE} , V_{CE} , T_j , that is,

$$I_C = I_C(V_{BE}, V_{CE}, T_j) \quad (37)$$

If V_{BE} is kept constant, the variation of I_C due to small variations of V_{CE} and T_j (the latter dictated by variations of V_{CE} or T_B) is given by

$$dI_C = \frac{\partial I_C}{\partial V_{CE}} \cdot dV_{CE} + \frac{\partial I_C}{\partial T_j} \cdot dT_j \quad (38)$$

which, neglecting the Early effect, reduces to

$$dI_C \approx \frac{\partial I_C}{\partial T_j} \cdot dT_j \quad (39)$$

If dT_j is due to dT_B , (39) becomes

$$dI_C|_{V_{CE}} \approx \frac{\partial I_C}{\partial T_j} \cdot dT_j|_{V_{CE}} \quad (40)$$

while, if it is due to dV_{CE} ,

$$dI_C|_{T_B} \approx \frac{\partial I_C}{\partial T_j} \cdot dT_j|_{T_B} \quad (41)$$

The variation of the junction temperature due to a small variation of T_B is

$$dT_j|_{V_{CE}} = dT_B + R_{THB0} \cdot V_{CE} \cdot dI_C|_{V_{CE}} = dT_B + R_{THB0} \cdot V_{CE} \cdot \frac{\partial I_C}{\partial T_j} \cdot dT_j|_{V_{CE}} \quad (42)$$

where use has been made of (40). From (42), it is obtained that

$$dT_j|_{V_{CE}} = \frac{dT_B}{1 - R_{THB0} \cdot V_{CE} \cdot \frac{\partial I_C}{\partial T_j}} \quad (43)$$

The variation of the junction temperature due to a small variation of V_{CE} is ($dT_B = 0$ K)

$$dT_j|_{T_B} = R_{THB0} \cdot (I_C \cdot dV_{CE} + dI_C|_{T_B} \cdot V_{CE}) = R_{THB0} \cdot \left(I_C \cdot dV_{CE} + \frac{\partial I_C}{\partial T_j} \cdot dT_j|_{T_B} \cdot V_{CE} \right) \quad (44)$$

by exploiting (41). From (44),

$$dT_j|_{T_B} = \frac{R_{THB0} \cdot I_C \cdot dV_{CE}}{1 - R_{THB0} \cdot V_{CE} \cdot \frac{\partial I_C}{\partial T_j}} \quad (45)$$

The base current I_B is a function of the independent variables V_{BE} , T_j , that is,

$$I_B = I_B(V_{BE}, T_j) \quad (46)$$

By considering that V_{BE} is constant,

$$dI_B = \frac{\partial I_B}{\partial T_j} \cdot dT_j \quad (47)$$

If dT_j is obtained through a variation dT_B , (47) becomes

$$dI_B|_{V_{CE}} = \frac{\partial I_B}{\partial T_j} \cdot dT_j|_{V_{CE}} \quad (48)$$

while, if it is induced by dV_{CE} ,

$$dI_B|_{T_B} = \frac{\partial I_B}{\partial T_j} \cdot dT_j|_{T_B} \quad (49)$$

Dividing (48) by (49) and making use of (43) and (45)

$$\frac{dI_B|_{V_{CE}}}{dI_B|_{T_B}} = \frac{dT_j|_{V_{CE}}}{dT_j|_{T_B}} = \frac{dT_B}{R_{THB0} \cdot I_C \cdot dV_{CE}} \quad (50)$$

from which

$$R_{THB0} = \frac{1}{I_C} \cdot \frac{\left. \frac{dI_B}{dV_{CE}} \right|_{T_B}}{\left. \frac{dI_B}{dT_B} \right|_{V_{CE}}} = \frac{1}{I_C} \cdot \frac{\frac{I_B(V_{BE}, V_{CE} + dV_{CE}, T_B) - I_B(V_{BE}, V_{CE}, T_B)}{dV_{CE}}}{\frac{I_B(V_{BE}, V_{CE}, T_B + dT_B) - I_B(V_{BE}, V_{CE}, T_B)}{dT_B}} \quad (51)$$

The technique can be easily extended to account for the Early effect, here omitted only to simplify the derivation; it suffices to multiply the denominator by $1 + V_{CE}/V_{AF}$, V_{AF} being the forward Early voltage.

The terms on the RHS can be obtained by measuring three I_B – V_{BE} characteristics at (V_{CE}, T_B) , $(V_{CE} + dV_{CE}, T_B)$, and $(V_{CE}, T_B + dT_B)$, and choosing a V_{BE} value that, concurrently with V_{CE} , ensures a low P_D but an appreciable self-heating. By repeating the process at various T_B , the experimental behavior of R_{THB0} vs. T_B is obtained; by comparing it with (9), if R_{TH00} has been measured, α is calibrated and then also used in (13).

3.5. Menozzi et al.

The technique developed by Menozzi et al. [48] allows the experimental extraction of R_{TH} as a function of T_B and P_D based on a couple of assumptions. The method requires the common-emitter measurements of various (seven can be enough [48]) I_C – V_{CE} characteristics at an assigned base current I_B for various T_B values, the lowest of which is referred to as T_{B0} . Let us denote as V_{CE0} the lowest V_{CE} applied under forward mode for all curves and as I_{C00} the collector current at V_{CE0} and $T_B = T_{B0}$. Lastly, let us call $P_{D0}(T_B)$ the dissipated powers corresponding to the V_{CE0} values for all characteristics. The first assumption of the method is that, for any assigned T_B , $R_{TH}(T_B, P_D)$ is a linearly increasing function of P_D , that is,

$$R_{TH}(T_B, P_D) = R_{TH}(T_B, P_{D0}(T_B)) + A_{Menozzi}(T_B) \cdot (P_D - P_{D0}(T_B)) \quad (52)$$

where the (positive) slope $A_{Menozzi}$ is a function of the applied T_B . The second assumption is that the collector current I_C linearly decreases with T_j (no matter how T_j is increased) for an assigned I_B , which is only true for HBTs due to the NTC of β_F . This can be expressed as

$$I_C(T_j) = I_{C00} \cdot [1 - \kappa \cdot (T_j - T_{j00Menozzi})] \quad (53)$$

$T_{j00Menozzi}$ being the junction temperature corresponding to V_{CE0} and T_{B0} , i.e.,

$$T_{j00Menozzi} = T_{B0} + R_{TH}(T_{B0}, P_{D00}) \cdot P_{D00} \approx T_{B0} + R_{TH}(T_{B0}, P_{D00}) \cdot V_{CE0} \cdot I_{C00} \quad (54)$$

where $P_{D0}(T_{B0})$ has been denoted as P_{D00} . Let us subtract (54) from (1)

$$\begin{aligned} T_j - T_{j00Menozzi} &= T_B - T_{B0} + R_{TH}(T_B, P_D) \cdot P_D - R_{TH}(T_{B0}, P_{D00}) \cdot P_{D00} = \\ &= T_B - T_{B0} + [R_{TH}(T_B, P_{D0}(T_B)) + A_{Menozzi}(T_B) \cdot (P_D - P_{D0}(T_B))] \cdot P_D - R_{TH}(T_{B0}, P_{D00}) \cdot P_{D00} \end{aligned} \quad (55)$$

where use has been made of (52). By substituting the RHS of (55) into (53),

$$I_C(T_j) = a_2(T_B) \cdot P_D^2 + a_1(T_B) \cdot P_D + a_0(T_B) \quad (56)$$

with

$$\begin{aligned} a_0(T_B) &= I_{C00} \cdot \{1 - \kappa \cdot [T_B - T_{B0} - R_{TH}(T_{B0}, P_{D00}) \cdot P_{D00}]\} = \\ &= -\kappa \cdot I_{C00} \cdot T_B + I_{C00} + \kappa \cdot I_{C00} \cdot T_{B0} + \kappa \cdot I_{C00} \cdot R_{TH}(T_{B0}, P_{D00}) \cdot P_{D00} = \\ &= B_{Menozzi} \cdot T_B + C_{Menozzi} \end{aligned} \quad (57)$$

$$a_1(T_B) = -\kappa \cdot I_{C00} \cdot [R_{TH}(T_B, P_{D0}(T_B)) - A_{Menozzi}(T_B) \cdot P_{D0}(T_B)] \quad (58)$$

$$a_2(T_B) = -\kappa \cdot I_{C00} \cdot A_{Menozzi}(T_B) \quad (59)$$

Hence, $I_C(T_j)$ is expressed as a function of T_B and P_D in any point of the measured curves.

As a next step, the I_C - P_D curves associated to the I_C - V_{CE} ones are determined by a simple elaboration of the data. Then, the values of coefficients a_0 , a_1 , a_2 favoring the best agreement between the experimental I_C - P_D curves and (56) can be found for each T_B with a 2nd-order polynomial fit, and the three a_0 - T_B , a_1 - T_B , a_2 - T_B characteristics are available. By comparing the a_0 - T_B curve and (57), $B_{Menozzi}$ and $C_{Menozzi}$ can be calibrated. Hence, κ is evaluated as

$$\kappa = -\frac{B_{Menozzi}}{I_{C00}} \quad (60)$$

and the thermal resistance $R_{TH}(T_{B0}, P_{D00})$ as

$$R_{TH}(T_{B0}, P_{D00}) = \frac{\frac{C_{Menozzi}}{I_{C00}} - \kappa \cdot T_{B0} - 1}{\kappa \cdot P_{D00}} \quad (61)$$

From (59), $A_{Menozzi}(T_B)$ is obtained for each T_B as

$$A_{Menozzi}(T_B) = -\frac{a_2(T_B)}{\kappa \cdot I_{C00}} \quad (62)$$

Consequently, from (58), $R_{TH}(T_B, P_{D0}(T_B))$ can be determined as

$$R_{TH}(T_B, P_{D0}(T_B)) = A_{Menozzi}(T_B) \cdot P_{D0}(T_B) - \frac{a_1(T_B)}{\kappa \cdot I_{C00}} \quad (63)$$

Once $A_{Menozzi}(T_B)$ and $R_{TH}(T_B, P_{D0}(T_B))$ are known, the linear R_{TH} vs. P_D increase for each T_B as given by (52) is achieved.

Although this technique is suited for HBTs, it can in principle also be applied to Si BJTs by assuming a linear increase of I_C with T_j in (53). However, in the presence of significant Early effect, which is not accounted for, the extracted thermal resistance will be overestimated.

3.6. Berkner and Balanethiram et al.

The technique of Berkner [55], subsequently also presented by Balanethiram et al. [15], belongs to the category of approaches based on intersection(s) between curves and does not rely on a thermometer. Under forward active mode, at V_{BE} not too high to avoid Kirk and resistive effects, if the Early effect is negligible and V_{CE} (V_{CB}) is sufficiently low to avoid avalanche, the collector current is given by

$$I_C(V_{BE}, T_j) = I_S(T_j) \cdot \exp\left(\frac{V_{BE}}{V_T}\right) \quad (64)$$

The technique requires the measurement of two V_{CE} -constant I_C - V_{BE} characteristics, the first obtained by assigning (V_{CE1}, T_{B1}) , and the second fixing (V_{CE2}, T_{B2}) , where $V_{CE1} < V_{CE2}$ and $T_{B1} > T_{B2}$. For low V_{BE} values (low self-heating), the junction temperature T_{j1} along the (V_{CE1}, T_{B1}) curve will be higher than T_{j2} associated to the (V_{CE2}, T_{B2}) counterpart, as $T_{B1} > T_{B2}$ dominates with respect to $P_{D1} < P_{D2}$, that is, invoking (1),

$$T_{j1} > T_{j2} \Leftrightarrow T_{B1} + R_{TH}(T_{B1}, P_{D1}) \cdot P_{D1} > T_{B2} + R_{TH}(T_{B2}, P_{D2}) \cdot P_{D2} \quad (65)$$

On the other hand, by increasing V_{BE} , P_{D2} grows faster than P_{D1} , thus leading to

$$T_{j1} < T_{j2} \Leftrightarrow T_{B1} + R_{TH}(T_{B1}, P_{D1}) \cdot P_{D1} < T_{B2} + R_{TH}(T_{B2}, P_{D2}) \cdot P_{D2} \quad (66)$$

As a result, there will be a value of V_{BE} where $T_{j1} = T_{j2}$, that is,

$$T_{B1} + R_{TH}(T_{B1}, P_{D1}) \cdot P_{D1} = T_{B2} + R_{TH}(T_{B2}, P_{D2}) \cdot P_{D2} \quad (67)$$

This V_{BE} value can be easily identified as the one at which the two characteristics intersect, as in the assumption of validity of (64), $T_{j1} = T_{j2}$ also implies $I_{C1} = I_{C2}$ and therefore $V_{BE1} = V_{BE2}$. Here Berkner and Balanethiram et al. assume that $R_{TH}(T_{B1}, P_{D1}) = R_{TH}(T_{B2}, P_{D2}) = R_{TH}$, and evaluate R_{TH} from (67) as

$$R_{TH} = \frac{T_{B1} - T_{B2}}{P_{D2} - P_{D1}} \quad (68)$$

and the corresponding $T_j = T_{j1} = T_{j2}$ from either the LHS or RHS of (67). By repeating the procedure for different (V_{CE}, T_B) couples, they determine the R_{TH} vs. T_j behavior.

Although this technique is quite easy to apply, it is affected by some drawbacks. First, the authors seem to claim that R_{TH} is only dependent on T_j ; however, the theory presented in Section 2 (Figure 1b) clearly demonstrates that R_{TH} is *not* univocally determined by T_j , but separately depends on T_B and P_D . For this reason, we think that the equality $R_{TH}(T_{B1}, P_{D1}) = R_{TH}(T_{B2}, P_{D2})$ and the extracted R_{TH} – T_j behavior are questionable. In addition, the intersection point must be taken where the Kirk effect does not play a role to prevent I_C from being V_{CB} dependent. Lastly, the method cannot be applied to Si BJTs, where the collector current would depend on V_{CE} also due to the Early effect.

3.7. Huszka et al.

Huszka and his co-workers [17] present an improved variant of the technique from Berkner [55] to account for the separate dependence of R_{TH} on T_B and P_D . They recast (67) as

$$\frac{T_{B1} - T_{B2}}{P_{D2} - P_{D1}} = \frac{R_{TH}(T_{B2}, P_{D2}) \cdot P_{D2}}{P_{D2} - P_{D1}} - \frac{R_{TH}(T_{B1}, P_{D1}) \cdot P_{D1}}{P_{D2} - P_{D1}} \quad (69)$$

where the LHS is the original Berkner's thermal resistance given by (68). Then they propose to use (13) or the linearized (17) for $R_{TH}(T_{B1}, P_{D1})$ and $R_{TH}(T_{B2}, P_{D2})$, so that (69) becomes an equation with two unknowns, i.e., R_{TH00} and α . The authors find many intersection points by varying V_{CE} and T_B ; by using (69) for each point, an equation system with unknowns R_{TH00} and α is obtained. Subsequently, α (given as an input) is varied in a reasonably wide range, and parameter R_{TH00} is optimized for each α ("single-variable optimization"); the (input) α and the calibrated R_{TH00} ensuring the minimum sum of the squared differences between LHS and RHS of all the system are finally selected.

Differently from [45,50], and similar to [29,47,48], here the analytical R_{TH} dependences on T_B and P_D are imposed by the technique. Conveniently, in Section 4 a numerical analysis will allow demonstrating that (13) or (17) with calibrated parameters favor a good agreement with realistic $R_{TH}(T_B, P_D)$ data, regardless of the technology.

The need to find many intersection points between I_C – V_{BE} characteristics at different V_{CE} and T_B values in a well-defined range (see Section 3.6) seems to be a shortcoming of this approach.

Lastly, it is important to remark that also other techniques, not specifically conceived to extract the influence of nonlinear thermal effects on R_{TH} , can in principle be exploited to determine the R_{THB0} vs. T_B behavior at low P_D . An example is given by the thermometer-based method proposed by d'Alessandro et al. [13] and its enriched variant accounting for the Early effect [14,56], which are slightly less straightforward, yet more robust, than "differential" methods or approaches based on the *direct* adoption of the V_{BE} – T_j thermometer to determine T_j from the measured V_{BE} . The technique is articulated as follows: (1) the slope $\phi(I_E)$ of the V_{BE} – T_B curve is extracted at various I_E sufficiently small to avoid self-heating (so that $T_j \approx T_B$); (2) an analytical model for the ϕ dependence on I_E (valid also for I_E values entailing self-heating) is determined and verified; (3) R_{TH} is calculated from $\phi(I_E)$ and the slope of an I_E -constant V_{BE} – V_{CB} characteristic (or equivalently from the slope of the corresponding V_{BE} – P_D curve) at dissipated power sufficiently high to favor self-heating, but low enough to avoid the nonlinear self-heating effect. Step (3) can be then repeated at various backside temperatures T_B . Unfortunately, it is not possible to evaluate the influence

of the nonlinear self-heating effect on R_{TH} , as P_D is varied in an assigned range during a single extraction.

The main features of the presented techniques are summarized in Table 2.

Table 2. Main features of the experimental R_{TH} extraction techniques explicitly accounting for nonlinear thermal effects.

Technique	R_{TH} Extraction Procedure	Advantages, Approximations, and Limitations
Bovolon et al. [50]	R_{TH} is experimentally extracted as a function of T_B and P_D with an extended version of the approach in [51]. For each (T_B, P_D) couple, two I_B -constant I_C - V_{CE} (and the related V_{BE} - V_{CE}) characteristics at T_B and $T_B + \Delta T_B$ have to be measured.	The technique allows extracting $R_{TH}(T_B, P_D)$ without any analytical assumption on the dependence of R_{TH} on T_B and P_D . However, the (T_B, P_D) , $(T_B, P_D + \Delta P_D)$, $(T_B + \Delta T_B, P_D)$ couples needed for the evaluation of ϕ and $R_{TH}(T_B, P_D)$ must be cautiously selected. Moreover, the approach is “differential”, being based on differences between two V_{BE} values, and thus it may suffer from a relatively high inaccuracy.
Yeats [45]	R_{TH} is experimentally extracted as a function of T_B and P_D with an improved version of the approach in [51]. It requires the measurement of some I_E -constant V_{BE} - V_{CE} characteristics at various T_B values.	The technique allows extracting $R_{TH}(T_B, P_D)$ without any assumption on the dependence of R_{TH} on T_B and P_D . Questionable points are the accuracy of the extrapolation step needed to calibrate the V_{BE} - T_j thermometer, and the <i>direct</i> use of the thermometer to evaluate T_j for each V_{BE} , which makes the extracted T_j (and the related R_{TH}) too sensitive to the precision in the V_{BE} measurements.
Marsh [47]	R_{THB0} is experimentally extracted as a function of T_B at low power. The technique requires the measurement of three I_B -constant I_C - V_{CE} characteristics at different T_B values.	A linear increase of R_{THB0} on T_B is assumed. The P_D dependence of R_{TH} is not considered.
Paasschens et al. [29]	R_{THB0} is experimentally extracted as a function of T_B at low power by resorting to the approach in [54], which for each T_B requires the measurement of three I_B - V_{BE} characteristics.	The technique does not extract the P_D dependence of R_{TH} , and uses only low-power data to optimize parameter α to be applied in (13). In addition, the “differential” approach in [54] may suffer from a significant inaccuracy if not carefully applied.
Menozi et al. [48]	R_{TH} is experimentally extracted as a function of T_B and P_D . The technique requires the measurements of some I_B -constant I_C - V_{CE} characteristics by varying T_B .	A linear behavior of $R_{TH}(T_B, P_D)$ on P_D with a T_B -sensitive slope is assumed. The dependence of I_C (β_F) on T_j under I_B -constant conditions is assumed to be linear, while being exponential. Lastly, the technique cannot be applied to Si BJTs with significant Early effect.
Berkner [55] and Balanethiram et al. [15]	R_{TH} is experimentally extracted as a function of T_j by identifying the intersection point between two I_C - V_{BE} curves at different couples (V_{CE1}, T_{B1}) and (V_{CE2}, T_{B2}) with $V_{CE1} < V_{CE2}$ and $T_{B1} > T_{B2}$.	The technique is intrinsically affected by the assumption that R_{TH} is only a function of T_j , while it can assume different values for a given T_j , depending on T_B . The intersection point should be taken in a region where the Kirk effect does not occur. The method cannot be applied to Si BJTs with significant Early effect.
Huszka [17]	It is an improved variant of Berkner’s method [55]. It imposes (13) or the linearized (17) to describe the separate dependence of R_{TH} on T_B and P_D . It requires the measurements of several I_C - V_{BE} curves at various V_{CE} and T_B values.	Reliable values for parameters R_{TH00} and α in (13) or (17) can be achieved by applying an optimization procedure to many intersection points determined as proposed by Berkner [55].

4. Numerical Simulation

In this Section, we resort to extremely detailed COMSOL [57] 3-D static finite-element method (FEM) thermal simulations of an InGaP/GaAs NPN HBT and a Si/SiGe NPN HBT chosen as well-representative case studies. For both devices, the thermal resistances R_{TH} were evaluated over reasonably wide ranges of T_B and P_D by activating the temperature

dependence of the thermal conductivities. This simulation study is intended to *emulate* the results of experimental extraction techniques like [45,50], which do not impose any analytical dependence of R_{TH} on T_B or P_D . The data were used to test the accuracy of the single-semiconductor formulations introduced earlier to describe $R_{TH}(T_B, P_D)$.

4.1. Devices under Test

The InGaP/GaAs NPN HBT is a mesa-isolated device manufactured by Qorvo, the key features of which are reported in Table 3. The transistor cell consists of four emitter fingers, each with $2 \times 20.5 \mu\text{m}^2$ area (the total emitter area then amounts to $164 \mu\text{m}^2$). The GaAs substrate is $620\text{-}\mu\text{m}$ thick and equipped with $65 \times 65 \mu\text{m}^2$ pads in a ground-signal-ground configuration for bare-die experimental characterization through RF probes. Further technological details are provided in [10].

Table 3. Key features of the InGaP/GaAs NPN HBT under test.

Parameter	Value
Common-emitter current gain β_F at 300 K and medium current levels	135
Open-emitter breakdown voltage BV_{CBO}	27 V
Open-base breakdown voltage BV_{CEO}	17 V
Peak cut-off frequency f_T for $V_{CE} = 3$ V	40 GHz
Collector current density J_C at peak f_T for $V_{CE} = 3$ V	$0.2 \text{ mA}/\mu\text{m}^2$
Maximum oscillation frequency f_{MAX} for $V_{CE} = 3$ V	82 GHz

The Si/SiGe NPN HBT was fabricated by Infineon Technologies AG in the framework of the European project DOTFIVE. The device, whose figures of merit are listed in Table 4, has only one base and one collector contact (BEC configuration), and belongs to the latest project technology stage, also denoted as set #3 in [13,14]. The drawn emitter area is equal to $0.2 \times 2.8 \mu\text{m}^2$, and the substrate is $185\text{-}\mu\text{m}$ thick.

Table 4. Key features of the Si/SiGe NPN HBT under test.

Parameter	Value
Common-emitter current gain β_F at 300 K and medium current levels	1500
Open-emitter breakdown voltage BV_{CBO}	5.5 V
Open-base breakdown voltage BV_{CEO}	1.6 V
Peak cut-off frequency f_T for $V_{CB} = 0.5$ V	240 GHz
Collector current density J_C at peak f_T for $V_{CB} = 0.5$ V	$10 \text{ mA}/\mu\text{m}^2$
Maximum oscillation frequency f_{MAX} for $V_{CB} = 0.5$ V	380 GHz

The 3-D geometries and the meshes of the devices under test in the COMSOL environment are displayed in Figures 2 and 3. The unique accuracy in emulating the real structure of the transistors was obtained by virtue of an *in-house* routine relying on the MATLAB-COMSOL Livelink [9]. In both technologies, the heat source was considered to geometrically coincide with the base-collector space-charge region. An isothermal boundary condition at temperature T_B was applied to the substrate backside, while the lateral sides and the top surface were assumed adiabatic. The mesh of the InGaP/GaAs HBT presents 2.8×10^6 tetrahedra and 3.6×10^6 degrees of freedom, while that of the Si/SiGe HBT involves 1.7×10^6 tetrahedra and 3.9×10^6 degrees of freedom. The thermal conductivities of the ternary alloys $\text{In}_x\text{Ga}_{1-x}\text{P}$ and $\text{In}_x\text{Ga}_{1-x}\text{As}$ (for the emitter of the InGaP/GaAs HBT), as well as of the binary alloy $\text{Si}_{1-x}\text{Ge}_x$ (for the base of the Si/SiGe HBT), x being the mole fraction of In (in the GaP or GaAs lattice) and Ge (in the Si lattice), were calculated using formulas available in [22]. For the Si/SiGe HBT, two additional conductivity degradation effects were included, namely, one dictated by the high phonon-impurity scattering in

the highly doped regions, and another induced by the phonon scattering with lateral boundaries in narrow layers, like emitter tungsten contact, Si emitter, SiGe base, and Si volume embraced by the shallow trench [14]. The CPU time required for each nonlinear static simulation was about 5–10 min using a PC equipped with an AMD Ryzen 5 3600 and 16 GB of RAM.

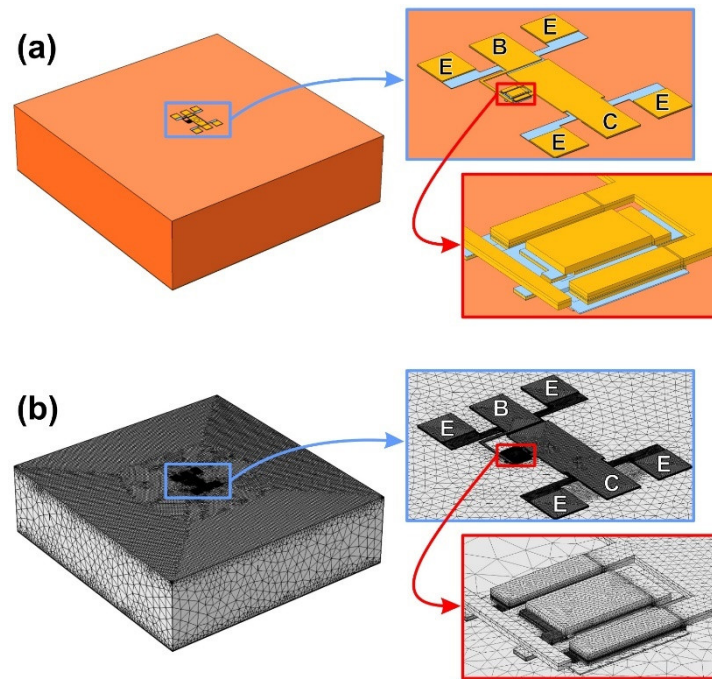


Figure 2. COMSOL environment: (a) geometry of the InGaP/GaAs HBT under test and (b) corresponding mesh.

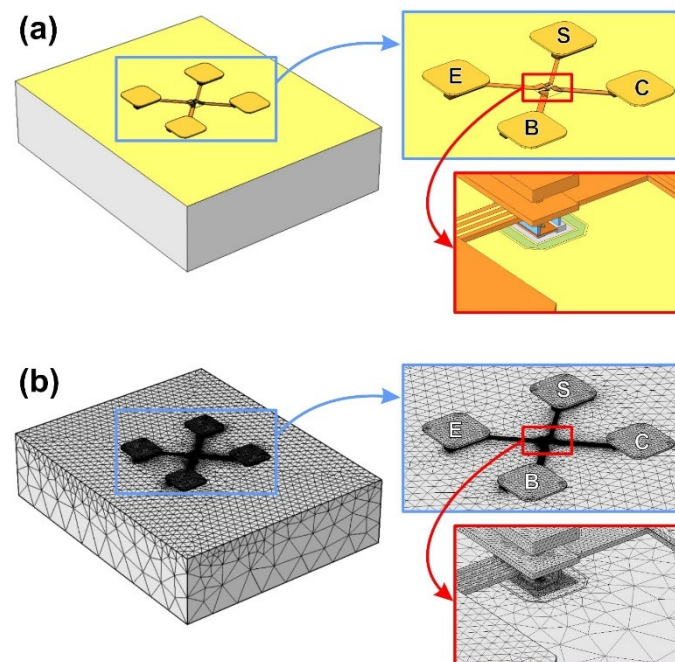


Figure 3. COMSOL environment: (a) geometry of the Si/SiGe HBT under test and (b) related mesh.

4.2. Results

By making use of the aforementioned simulation strategy, the $T_B = T_0$ zero-power thermal resistances R_{TH0} were found to be 457.6 K/W for the InGaP/GaAs HBT, and 6829 K/W

for the Si/SiGe HBT, values very close to the experimental counterparts determined with the methods in [51] for the InGaP/GaAs HBT and [13,14] for the Si/SiGe HBT.

The simulated R_{TH} vs. P_D curves for various T_B values are shown in Figure 4.

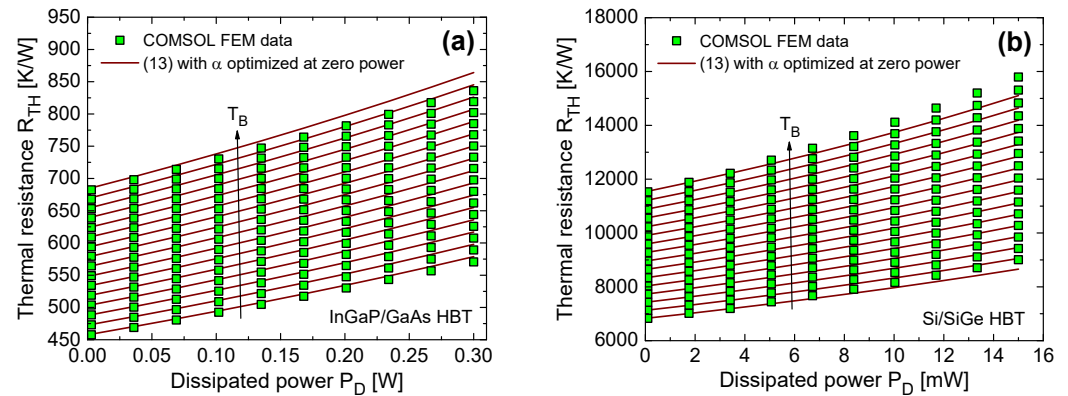


Figure 4. R_{TH} vs. P_D for T_B spanning the range 300 to 450 K for (a) the InGaP/GaAs HBT and (b) the Si/SiGe HBT. COMSOL data (symbols) are compared with (13) where α was calibrated at very low dissipated power (solid brown lines), as shown in Figure 5.

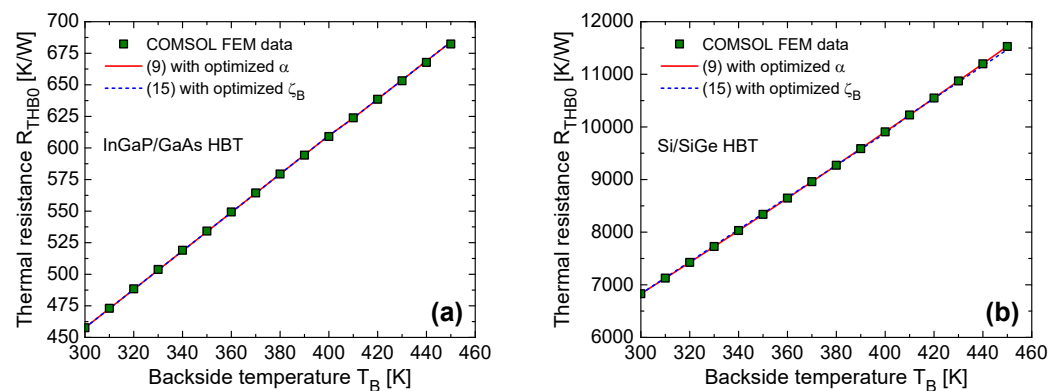


Figure 5. Zero-power thermal resistance R_{TH0} as a function of T_B for (a) the InGaP/GaAs HBT and (b) the Si/SiGe HBT. COMSOL data (symbols) are compared to (9) with optimized α (solid red line) and (15) with calibrated ζ_B (dashed blue line).

A first investigation was aimed at testing the accuracy of the R_{TH0} vs. T_B formulations, namely, the power (9) and linear (15) laws with parameters α and ζ_B optimized by means of a simple code performing a least squares fitting. Figure 5 shows the results. For the InGaP/GaAs HBT, (9) with $\alpha = 0.99$ and (15) with $\zeta_B = 3.3 \times 10^{-3} \text{ K}^{-1}$ almost provide the same accuracy, while for the Si/SiGe HBT, (9) with $\alpha = 1.2924$ is slightly better than (15) with $\zeta_B = 4.53 \times 10^{-3} \text{ K}^{-1}$.

Unfortunately, we found that the α value calibrated at zero power cannot be used to accurately account for the nonlinear self-heating effect through (13), as proposed in [29]. Figure 4 witnesses that $\alpha = 0.99$ leads to an overestimation of R_{TH} at medium/high dissipated power for the InGaP/GaAs HBT, while $\alpha = 1.2924$ gives rise to an underestimation for the Si/SiGe HBT.

Then we tested the modeling approach suggested by Yeats [45] that requires a “brute-force 2-D search” of the R_{TH0} and α values ensuring the best agreement between *all* COMSOL R_{TH} data and (13). In this case, R_{TH0} is not the COMSOL (or equivalently the experimental) $T_B = T_0$ zero-power thermal resistance, but becomes a parameter to calibrate. For the InGaP/GaAs HBT, the optimization led to $R_{TH0} = 459.4 \text{ K/W}$ (with a 0.39% discrepancy with respect to the COMSOL value) and $\alpha = 0.951$, while for the Si/SiGe HBT, $R_{TH0} = 6855.8 \text{ K/W}$ (0.39%) and $\alpha = 1.333$. Figure 6 shows that the resulting agreement between the COMSOL thermal resistances and (13) is very good for both technologies. This

is an important result, as it demonstrates that the R_{TH} dependence on T_B and P_D of a *real* bipolar transistor, independently of the technology, can be accurately described with the simple single-semiconductor theory by calibrating two parameters only, namely, R_{TH00} and α ; in addition, R_{TH00} does not lose its physical meaning since the optimized value is very close to the reference (COMSOL) one.

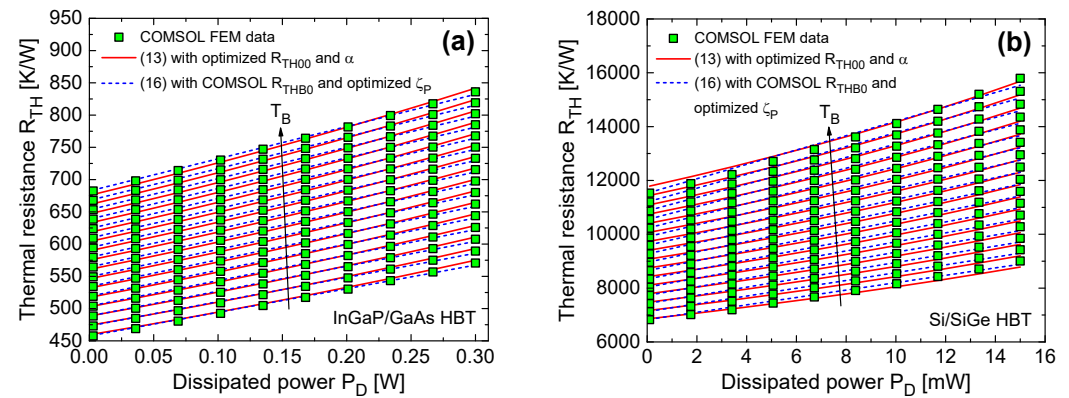


Figure 6. R_{TH} vs. P_D with T_B spanning the range 300 to 450 K for (a) the InGaP/GaAs HBT and (b) the Si/SiGe HBT. COMSOL data (symbols) are compared with (13) where R_{TH00} and α were optimized through a “brute-force 2-D search” carried out over all the simulated R_{TH} values (solid red lines), and with (16) using the R_{THB0} vs. T_B values determined by COMSOL and ζ_P calibrated at each T_B (dashed blue lines).

We also examined the accuracy of the linearized formulation (16). Adopting (16) with (9) for R_{THB0} and the R_{TH00} and α values calibrated with the “brute-force 2-D search” leads to a perceptible underestimation of COMSOL data at medium/high P_D (not shown in the figures). Instead, (16) reaches a level of accuracy comparable with (13) only using (9) for R_{THB0} with the COMSOL (or equivalently the experimental) R_{TH00} and α calibrated on low-power data, and optimizing coefficient ζ_P (which can be used as a model parameter in compact transistor models) at each T_B . In our analysis, we did not calibrate α in (9) on low-power data, as the R_{THB0} values corresponding to each T_B were all available from COMSOL simulations. It was found that the optimized ζ_P slightly decreases for the InGaP/GaAs HBT (from 0.8 W^{-1} at $T_B = T_0 = 300 \text{ K}$ to 0.733 W^{-1} at $T_B = 450 \text{ K}$) and marginally increases for the Si/SiGe HBT (from 20.09 W^{-1} to 23.16 W^{-1}). The resulting R_{TH} vs. P_D curves are also shown in Figure 6.

5. R_{TH} Formulations Available in Compact Transistor Models and Update

In compact models of bipolar transistors accounting for self-heating, namely, VBIC [58], Mextram 504 [59], Agilent HBT (AHBT) [60], and HICUM [61,62], all available in Keysight ADS [63], the power-temperature feedback is implemented through an *equivalent thermal network*, i.e., an electrical circuit where currents, voltages, resistances, and capacitances represent dissipated powers, temperatures, thermal resistances, and thermal capacitances, respectively. More specifically, in VBIC, Mextram 504, and HICUM, the default network is the one depicted in Figure 7a, while in AHBT it is the one shown in Figure 7b. Conveniently, all these models are equipped with an externally accessible thermal node that allows the implementation of a thermal network in any form.

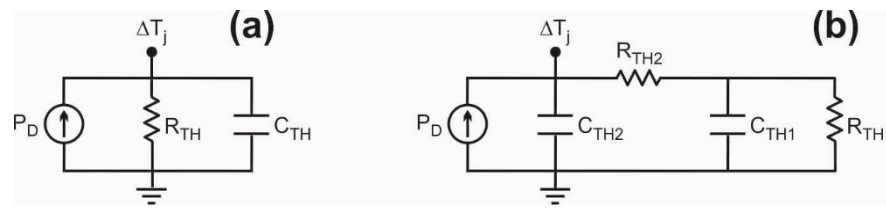


Figure 7. Equivalent thermal network included (a) in VBIC, Mextram 504, HICUM, and (b) in AHBT.

5.1. VBIC

In VBIC, R_{TH} is assumed to be a constant parameter, that is, nonlinear thermal effects are not captured. This is problematic when simulating ET effects at medium/high junction temperatures.

5.2. Mextram 504

Mextram 504 implements the impact of backside (or ambient) temperature on R_{TH} according to

$$R_{TH} = R_{TH} \cdot \left(\frac{273.15 + TEMP}{273.15 + TREF} \right)^{ATH} \quad (70)$$

where $TREF$ (default: 25 °C) is the reference temperature at which parameters are extracted, $TEMP$ (default: 25 °C) is the ambient temperature defined at the device instance, R_{TH} (default: 300 K/W) and ATH (default: 0, although a list of suitable values for the most important materials is provided in [59]) are model parameters. Unfortunately, although the Mextram 504 team was well aware of the influence of the nonlinear self-heating effect on R_{TH} [29], this is not taken into account in the present release, as also correctly stated in [17]. Such a choice was probably made to ensure unconditional simulation stability at the price of a reduced accuracy at high P_D . By using the nomenclature introduced in Section 2, and considering that $273.15 + TREF \approx T_0$, $273.15 + TEMP = T_B$, and that R_{TH} and ATH coincide with R_{TH00} and α , (9) is obtained.

5.3. AgilentHBT (AHBT)

AgilentHBT (AHBT) implements the following R_{TH} model (Figure 7b):

$$R_{TH} = R_{TH1} + R_{TH2} = R_{TH1} \cdot \left(\frac{273.15 + Tdev}{273.15 + Tnom} \right)^{XTH1} + R_{TH2} \cdot \left(\frac{273.15 + Tdev}{273.15 + Tnom} \right)^{XTH2} \quad (71)$$

where $Tnom$ (default: 25 °C) is the nominal temperature at which parameters are extracted, R_{TH1} (default: 1000 K/W), $XTH1$ (default: 0), R_{TH2} (default: 0 K/W), $XTH2$ (default: 0) are model parameters, and $Tdev$ [°C] is the device temperature, given by

$$Tdev = Temp + \Delta T_j \quad (72)$$

In (72), $Temp$ (default: 25 °C) is the ambient temperature defined at the device instance, and ΔT_j (ΔT_j in Figure 7b) is dynamically calculated as

$$\Delta T_j = (R_{TH1} + R_{TH2}) \cdot P_D = R_{TH} \cdot P_D \quad (73)$$

Let us now use the nomenclature introduced in Section 2. By considering that $273.15 + Tnom \approx T_0$, $273.15 + Temp = T_B$, and $Tdev = T_j$, (71) can be rewritten as

$$R_{TH} = R_{TH1} \cdot \left(\frac{T_B + \Delta T_j}{T_0} \right)^{XTH1} + R_{TH2} \cdot \left(\frac{T_B + \Delta T_j}{T_0} \right)^{XTH2} \quad (74)$$

which by default reduces to the two-parameter formulation

$$R_{TH} = R_{TH1} \cdot \left(\frac{T_B + \Delta T_j}{T_0} \right)^{XTH1} \quad (75)$$

5.4. HiCUM

In the 2.4 release of HiCUM/L2, the thermal resistance is evaluated as [17,62]

$$R_{TH} = rth \cdot [1 + alrth \cdot (Temp + \Delta T_j - Tnom)] \cdot \left(\frac{273.15 + Temp + \Delta T_j}{273.15 + Tnom} \right)^{zetarh} \quad (76)$$

where $Tnom$ (default: 27 °C) is the reference temperature at which parameters are determined, $Temp$ (default: 27 °C) is the ambient temperature defined at the device instance, rth (default: 0 K/W), $alrth$ (default: 0 K⁻¹), $zetarh$ (default: 0) are model parameters, and ΔT_j is dynamically computed as

$$\Delta T_j = R_{TH} \cdot P_D \quad (77)$$

Let us now adopt the nomenclature reported in Section 2. By considering that $273.15 + Tnom = T_0$ and $273.15 + Temp = T_B$, (76) can be rewritten as

$$R_{TH} = rth \cdot [1 + alrth \cdot (T_B + \Delta T_j - T_0)] \cdot \left(\frac{T_B + \Delta T_j}{T_0} \right)^{zetarh} \quad (78)$$

5.5. Proposed R_{TH} Modeling Approaches

Starting from the findings achieved in Section 4, we propose to resort to (13) with optimized R_{TH00} and α in compact bipolar transistor models. However, implementing R_{TH} as a nonlinear T_B - and P_D -dependent resistor according to (13) would lead to a markedly unphysical behavior under dynamic conditions, where R_{TH} will be directly affected by (even fast) P_D variations in time.

A first solution (denoted as #1) involves the use of (i) a constant resistor R_{THB0} in the single-pole network depicted in Figure 7a, the value of which can be preliminarily calculated with (9), or (ii) a nonlinear resistor R_{THB0} given by (9), and a behavioral block (e.g., a nonlinear voltage-controlled voltage source) converting $R_{THB0} \cdot P_D$ into ΔT_j , with T_j given by (11). Besides T_0 , two model parameters are needed: R_{THB0} and α in case (i), and R_{TH00} and α in case (ii). This approach was successfully used on simple SPICE-compatible InGaP/GaAs and Si/SiGe HBT models in [10] and [64], respectively.

A second solution (referred to as #2) is obtained by replacing P_D with ΔT_j in (12) using (1), which leads to

$$1 = \frac{T_B}{\Delta T_j} \cdot \left\{ \left[1 - (\alpha - 1) \cdot \frac{R_{THB0}}{R_{TH}(T_B, P_D)} \cdot \frac{\Delta T_j}{T_B} \right]^{\frac{-1}{\alpha-1}} - 1 \right\} \quad (79)$$

whence

$$R_{TH}(T_B, \Delta T_j) = R_{THB0} \cdot \frac{\alpha - 1}{1 - \left(\frac{T_B + \Delta T_j}{T_B} \right)^{-(\alpha-1)}} \cdot \frac{\Delta T_j}{T_B} \quad (80)$$

Then, in the network of Figure 7a, R_{TH} must be implemented with a nonlinear resistor given by (80), where R_{THB0} is again either considered a model parameter to be calculated in the pre-processing stage at the assigned T_B with (9), or computed in the compact model through (9). Option #2 reduces the number of nodes in the compact model compared with #1.

A third solution (designated as #3) is to exploit a nonlinear current source controlled by ΔT_j to force through the thermal resistance branch a power given by [29]

$$P_D = \frac{\Delta T_j}{R_{TH}(T_B, \Delta T_j)} = \frac{T_B}{R_{THB0}} \cdot \frac{1 - \left(\frac{T_B + \Delta T_j}{T_B} \right)^{-(\alpha-1)}}{\alpha - 1} \quad (81)$$

which can be easily obtained from (80). For R_{THB0} , the considerations expressed before still hold.

Solutions #1, #2, #3 provide the same ΔT_j under static conditions. Conversely, approach #1 behaves differently from #2, #3 under *dynamic* conditions: by considering the network in Figure 7a and assuming the same thermal capacitance C_{TH} , #1 leads to a time constant shorter than that of #2 and #3, i.e., it gives rise to a faster response to a power step. Unfortunately, all approaches are expected to be inaccurate in describing the dynamic thermal behavior, mainly due to the simplicity of the single-pole model. A thermal network correctly accounting for nonlinear dynamic thermal effects has been presented in [65]; however, it is far more complex than the single-pole network used by default in VBIC, AHB, HICUM and can only be derived from a detailed 3-D thermal model of the device under test.

A simplified, yet slightly less accurate, option (called #4) uses the linearized dependence on P_D given by (16). Here, again P_D must be substituted with ΔT_j , which leads to the following R_{TH} formulation:

$$R_{TH}(T_B, \Delta T_j) = \frac{R_{THB0}}{2} \cdot \left(1 + \sqrt{1 + 2 \frac{\alpha}{T_B} \cdot \Delta T_j} \right) \quad (82)$$

or equivalently

$$R_{TH}(T_B, \Delta T_j) = \frac{R_{THB0}}{2} \cdot \left(1 + \sqrt{1 + 4 \frac{\zeta_P(T_B)}{R_{THB0}} \cdot \Delta T_j} \right) \quad (83)$$

in turn representing the linearized version of (80). In this case, R_{TH} in the thermal network of Figure 7a must be implemented as a nonlinear resistor given by (82). Owing to the findings obtained before, using (82) with R_{TH00} and α optimized through the “brute-force 2-D search” underestimates R_{TH} at medium/high ΔT_j ; a fairly good level of accuracy can instead be achieved by using (83) with ζ_P as a model parameter optimized at each T_B , or equivalently (82) with α optimized at each T_B .

It is worth noting that, apart from T_0 , all the above solutions make use of two parameters only, namely, R_{THB0} and α , if R_{THB0} is calculated in the preprocessing stage, or R_{TH00} and α , if R_{THB0} is expressed with (9) in the compact model. In the latter case, the computational burden can be alleviated by exploiting the linearized (15), which does not significantly reduce the accuracy.

Unfortunately, the R_{TH} formulations (75) and (78) employed in AHB and HICUM, respectively, do not allow obtaining a favorable match with the accurate single-semiconductor theory. By setting R_{TH1} in (75) and R_{TH} in (78) equal to the R_{TH00} value simulated by COMSOL, the R_{TH} vs. ΔT_j behavior determined by (75) and (78) strongly disagree with that corresponding to (80), independently of the choice of parameters X_{TH1} in (75) or alr_{th} and $zeta_{ar_{th}}$ in (78). In conclusion, the available thermal networks embedded in compact transistor models either do not consider or improperly account for nonlinear thermal effects. Hence, one of the implementations of the single-semiconductor theory (#1 to #4) should be suggested for their future releases.

Lastly, it is important to remark that all the results obtained with the simulation and modeling analyses performed in Sections 4 and 5 can be safely extended down to $T_B = 250$ K since the adopted laws for the thermal conductivities of all materials are still approximately valid in the range 250 to 300 K.

6. Conclusions

This paper is intended to offer a comprehensive overview of nonlinear thermal effects in bipolar transistors from a manifold perspective. In particular, the work includes: (i) a theoretical discussion on the underlying physics and an analytical model for the influence of such effects on the thermal resistance, rigorously valid only for an ideal, very simple device homogeneously composed of one semiconductor (*single-semiconductor assumption*); (ii) a critical review of the available experimental techniques to identify the impact of nonlinear

effects on the thermal resistance; (iii) a detailed 3-D numerical simulation campaign of state-of-the-art HBTs in InGaP/GaAs and Si/SiGe technologies, the results of which are exploited to verify the accuracy of the single-semiconductor theory; (iv) a description of the thermal resistance formulations embedded in the most relevant compact bipolar transistor models; (v) some proposals for the implementation of the single-semiconductor expressions in future releases of the compact models.

The main results can be summarized as follows.

- The theoretical analysis has allowed emphasizing a sometimes-overlooked aspect, i.e., that the thermal resistance suffers from two distinct nonlinear thermal effects associated with the backside temperature and dissipated power, and *cannot* be considered solely a function of the junction temperature.
- Only the techniques conceived by Bovolon et al. and Yeats allow the extraction of thermal resistance as a function of the backside temperature and dissipated power without imposing any analytical formulation for these dependences. However, the technique of Bovolon et al. is “differential” and thus prone to errors if not cautiously applied, while that of Yeats is based on a delicate and questionable thermometer calibration procedure.
- The detailed 3-D simulation campaign, performed to obtain realistic thermal resistance data as a function of backside temperature and dissipated power, has allowed demonstrating that the nonlinear thermal effects in a real transistor can be accurately described with the single-semiconductor approach if a proper parameter optimization is carried out.
- Conversely, the thermal resistance formulations used in the latest releases of compact bipolar transistor models for circuit simulators either do not include nonlinear thermal effects or improperly account for them. Some proposals for improving the implementation of such effects have been made, all inspired by the theory of the single-semiconductor device.

Author Contributions: Methodology, V.d.; software, V.d., A.P.C., C.S. and L.C.; investigation, V.d., M.M., M.S. and P.J.Z.; writing—original draft preparation, V.d.; writing—review and editing, V.d.; supervision, V.d., A.P.C., C.S., M.M., M.S. and P.J.Z. All authors have read and agreed to the published version of the manuscript.

Funding: Markus Müller and Michael Schröter acknowledge partial financial support from the German National Science Foundation (Deutsche Forschungsgemeinschaft), DFG project SCHR695/21. The funding for the Ph.D. activity of Ciro Scognamiglio was generously donated by the Rinaldi family in the memory of Niccolò Rinaldi, a bright Professor and Researcher of University of Naples Federico II, who prematurely passed away in 2018.

Institutional Review Board Statement: Not applicable.

Informed Consent Statement: Not applicable.

Data Availability Statement: Not applicable.

Acknowledgments: The authors wish to thank Klaus Aufinger for providing the technology/geometry details of the Si/SiGe HBT analyzed in the paper.

Conflicts of Interest: The authors declare no conflict of interest.

Nomenclature

β_F	common-emitter forward current gain
BV_{CBO}	open-emitter breakdown voltage [V]
BV_{CEO}	open-base breakdown voltage [V]
$\Delta T_j = T_j - T_B$	junction temperature rise over backside temperature [K]
f_{MAX}	maximum oscillation frequency [Hz]
f_T	unity-gain cut-off frequency (or transition frequency) [Hz]
I_B	base current [A]
I_C	collector current [A]
I_E	emitter current [A]
k	thermal conductivity [W/μmK]
P_D	dissipated power [W]
R_B	parasitic base series resistance [Ω]
R_E	parasitic emitter series resistance [Ω]
R_{TH} or $R_{TH}(T_B, P_D)$	self-heating thermal resistance [K/W]
$R_{TH00} = R_{TH}(T_B = T_0, P_D \rightarrow 0 \text{ W})$	self-heating thermal resistance at $T_B = T_0$ and a very low P_D (<i>ideally</i> for $P_D \rightarrow 0 \text{ W}$)
$R_{TH0P} = R_{TH}(T_B = T_0, P_D)$	self-heating thermal resistance at $T_B = T_0$ and an arbitrary P_D
$R_{THB0} = R_{TH}(T_B, P_D \rightarrow 0 \text{ W})$	self-heating thermal resistance at a generic T_B and a very low P_D (<i>ideally</i> for $P_D \rightarrow 0 \text{ W}$)
T_B	backside (or baseplate, or ambient) temperature [K]
T_j	average temperature of the base-emitter junction (<i>junction temperature</i>) at arbitrary T_B and P_D [K]
T_{j00}	junction temperature at $T_B = T_0$ and a very low P_D [K]
T_{j0P}	junction temperature at $T_B = T_0$ and an arbitrary P_D [K]
T_{jB0}	junction temperature at an arbitrary T_B and a very low P_D [K]
$T_0 = 300 \text{ K}$	reference temperature [K]
V_{AF}	forward Early voltage [V]
V_{BE}	externally applied base-emitter voltage [V]
$V_{BEj} = V_{BE} - R_B \cdot I_B - R_E \cdot I_E$	internal (or junction) base-emitter voltage [V]
V_{CB}	externally applied collector-base voltage [V]
V_{CE}	externally applied collector-emitter voltage [V]

Abbreviations

AlGaAs	ternary alloy formed by introducing a given mole fraction of aluminum (Al) in the place of Ga in the GaAs lattice
BJT	bipolar junction transistor
Cu	copper
ET	electrothermal
FEM	finite-element method
GaAs	gallium arsenide
GaN	gallium nitride
HBT	heterojunction bipolar transistor
InGaAs	ternary alloy created by introducing an assigned mole fraction of indium (In) in the place of Ga in the GaAs lattice
InGaP	ternary alloy formed by replacing a given mole fraction of Ga with indium (In) in the GaP lattice
InP	indium phosphide
NDR	negative differential resistance
NTC	negative temperature coefficient
PDR	positive differential resistance
PTC	positive temperature coefficient
Si	silicon
SiC	silicon carbide, with 4H-SiC and 6H-SiC polytypes
SiGe	silicon-germanium: binary alloy formed by substituting an assigned mole fraction of Si with germanium (Ge) in the Si lattice

References

1. Nenadović, N.; d'Alessandro, V.; Nanver, L.K.; Tamigi, F.; Rinaldi, N.; Slotboom, J.W. A back-wafer contacted silicon-on-glass integrated bipolar process—Part II: A novel analysis of thermal breakdown. *IEEE Trans. Electron Devices* **2004**, *51*, 51–62. [[CrossRef](#)]
2. Rinaldi, N.; d'Alessandro, V. Theory of electrothermal behavior of bipolar transistors: Part I—Single-finger devices. *IEEE Trans. Electron Devices* **2005**, *52*, 2009–2021. [[CrossRef](#)]

3. La Spina, L.; d'Alessandro, V.; Russo, S.; Rinaldi, N.; Nanver, L.K. Influence of concurrent electrothermal and avalanche effects on the safe operating area of multifinger bipolar transistors. *IEEE Trans. Electron Devices* **2009**, *56*, 483–491. [\[CrossRef\]](#)
4. Lee, C.-P.; Tao, N.G.M.; Lin, B.J.-F. Studies of safe operating area of InGaP/GaAs heterojunction bipolar transistors. *IEEE Trans. Electron Devices* **2014**, *61*, 943–949. [\[CrossRef\]](#)
5. Russo, S.; La Spina, L.; d'Alessandro, V.; Rinaldi, N.; Nanver, L.K. Influence of layout design and on-wafer heatspreaders on the thermal behavior of fully-isolated bipolar transistors: Part II—Dynamic analysis. *Solid-State Electron.* **2010**, *54*, 754–762. [\[CrossRef\]](#)
6. Liu, W.; Khatibzadeh, A. The collapse of current gain in multi-finger heterojunction bipolar transistors: Its substrate temperature dependence, instability criteria, and modeling. *IEEE Trans. Electron Devices* **1994**, *41*, 1698–1707. [\[CrossRef\]](#)
7. La Spina, L.; d'Alessandro, V.; Russo, S.; Nanver, L.K. Thermal design of multifinger bipolar transistors. *IEEE Trans. Electron Devices* **2010**, *57*, 1789–1800. [\[CrossRef\]](#)
8. Sevimli, O.; Parker, A.E.; Fattorini, A.P.; Mahon, S.J. Measurement and modeling of thermal behavior in InGaP/GaAs HBTs. *IEEE Trans. Electron Devices* **2013**, *60*, 1632–1639. [\[CrossRef\]](#)
9. d'Alessandro, V.; Catalano, A.P.; Codecasa, L.; Zampardi, P.J.; Moser, B. Accurate and efficient analysis of the upward heat flow in InGaP/GaAs HBTs through an automated FEM-based tool and Design of Experiments. *Int. J. Numer. Model.-Electron. Netw. Devices Fields* **2019**, *32*, e2530. [\[CrossRef\]](#)
10. d'Alessandro, V.; Catalano, A.P.; Scognamiglio, C.; Codecasa, L.; Zampardi, P.J. Analysis of electrothermal effects in devices and arrays in InGaP/GaAs HBT technology. *Electronics* **2021**, *10*, 757. [\[CrossRef\]](#)
11. d'Alessandro, V.; Marano, I.; Russo, S.; Céli, D.; Chantre, A.; Chevalier, P.; Pourchon, F.; Rinaldi, N. Impact of layout and technology parameters on the thermal resistance of SiGe:C HBTs. In Proceedings of the IEEE Bipolar/BiCMOS Circuits and Technology Meeting (BCTM), Austin, TX, USA, 4–6 October 2010; pp. 137–140.
12. Sahoo, A.K.; Frégonèse, S.; Weiß, M.; Malbert, N.; Zimmer, T. A scalable electrothermal model for transient self-heating effects in trench-isolated SiGe HBTs. *IEEE Trans. Electron Devices* **2012**, *59*, 2619–2625. [\[CrossRef\]](#)
13. d'Alessandro, V.; Sasso, G.; Rinaldi, N.; Aufinger, K. Influence of scaling and emitter layout on the thermal behavior of toward-THz SiGe:C HBTs. *IEEE Trans. Electron Devices* **2014**, *61*, 3386–3394. [\[CrossRef\]](#)
14. d'Alessandro, V.; Magnani, A.; Codecasa, L.; Rinaldi, N.; Aufinger, K. Advanced thermal simulation of SiGe:C HBTs including back-end-of-line. *Microelectron. Reliab.* **2016**, *67*, 38–45. [\[CrossRef\]](#)
15. Balanethiram, S.; Berkner, J.; D'Esposito, R.; Frégonèse, S.; Céli, D.; Zimmer, T. Extracting the temperature dependence of thermal resistance from temperature-controlled DC measurements of SiGe HBTs. In Proceedings of the IEEE Bipolar/BiCMOS Circuits and Technology Meeting (BCTM), Miami, FL, USA, 19–21 October 2017; pp. 94–97.
16. Balanethiram, S.; D'Esposito, R.; Frégonèse, S.; Chakravorty, A.; Zimmer, T. Validation of thermal resistance extracted from measurements on stripe geometry SiGe HBTs. *IEEE Trans. Electron Devices* **2019**, *66*, 4151–4155. [\[CrossRef\]](#)
17. Huszka, Z.; Nidhin, K.; Céli, D.; Chakravorty, A. Extraction of compact static thermal model parameters for SiGe HBTs. *IEEE Trans. Electron Devices* **2021**, *68*, 491–496. [\[CrossRef\]](#)
18. Rinaldi, N. Thermal analysis of solid-state devices and circuits: An analytical approach. *Solid-State Electron.* **2000**, *44*, 1789–1798. [\[CrossRef\]](#)
19. Pacelli, A.; Palestri, P.; Mastrapasqua, M. Compact modeling of thermal resistance in bipolar transistors on bulk and SOI substrates. *IEEE Trans. Electron Devices* **2002**, *49*, 1027–1033. [\[CrossRef\]](#)
20. Shanks, H.R.; Maycock, P.D.; Sidles, P.H.; Danielson, G.C. Thermal conductivity of silicon from 300 to 1400°K. *Phys. Rev.* **1963**, *130*, 1743–1748. [\[CrossRef\]](#)
21. Maycock, P.D. Thermal conductivity of silicon, germanium, III-V compounds and III-V alloys. *Solid-State Electron.* **1967**, *10*, 161–168. [\[CrossRef\]](#)
22. Palankovski, V.; Quay, R. *Analysis and Simulation of Heterostructure Devices*; Springer: New York, NY, USA, 2004.
23. Glassbrenner, C.J.; Slack, G.A. Thermal conductivity of silicon and germanium from 3°K to the melting point. *Phys. Rev.* **1964**, *134*, A1058–A1069. [\[CrossRef\]](#)
24. Lee, S.-S.; Allstot, D.J. Electrothermal simulation of integrated circuits. *IEEE J. Solid-State Circuits* **1993**, *28*, 1283–1293.
25. Wybourne, M.N. Thermal conductivity of Si. In *Properties of Silicon*; Emis Data Review Series; INSPEC: London, UK, 1988.
26. Bonani, F.; Ghione, G. On the application of the Kirchhoff transformation to the steady-state thermal analysis of semiconductor devices with temperature-dependent and piecewise inhomogeneous thermal conductivity. *Solid-State Electron.* **1995**, *38*, 1409–1412. [\[CrossRef\]](#)
27. Negus, K.J.; Franklin, R.W.; Yovanovich, M.M. Thermal modeling and experimental techniques for microwave bipolar devices. *IEEE Trans. Compon. Hybrids Manuf. Technol.* **1989**, *12*, 680–689. [\[CrossRef\]](#)
28. Walkey, D.J.; Smy, T.J.; Macelwee, T.; Maliepaard, M. Compact representation of temperature and power dependence of thermal resistance in Si, InP and GaAs substrate devices using linear models. *Solid-State Electron.* **2002**, *46*, 819–826. [\[CrossRef\]](#)
29. Paasschens, J.C.J.; Harmsma, S.; van der Toorn, R. Dependence of thermal resistance on ambient and actual temperature. In Proceedings of the IEEE Bipolar/BiCMOS Circuits and Technology Meeting (BCTM), Montreal, QC, Canada, 12–14 September 2004; pp. 96–99.
30. Blakemore, J.S. Semiconducting and other major properties of gallium arsenide. *J. Appl. Phys.* **1982**, *53*, R123–R181. [\[CrossRef\]](#)
31. Aliev, S.A.; Nashelskii, A.Y.; Shalyt, S.S. Thermal conductivity and thermoelectric power of N-type indium phosphide at low temperatures. *Sov. Phys. Solid State* **1965**, *7*, 1287.

32. Jaramillo-Fernandez, J.; Chavez-Angel, E.; Sanatinia, R.; Kataria, H.; Anand, S.; Lourdudoss, S.; Sotomayor-Torres, C.M. Thermal conductivity of epitaxially grown InP: Experiment and simulation. *CrystEngComm* **2017**, *19*, 1879–1887. [\[CrossRef\]](#)
33. Harris, G.L. *Properties of Silicon Carbide*; INSPEC: London, UK, 1995.
34. Goldberg, Y.; Levinshtein, M.R.; Rumyantsev, S.L. Silicon Carbide. In *Properties of Advanced Semiconductor Materials: GaN, AlN, InN, BN, SiC, SiGe*; Levinshtein, M.E., Rumyantsev, S.L., Shur, M.S., Eds.; John Wiley & Sons, Inc.: New York, NY, USA, 2001; Volume 5, pp. 93–148.
35. Joshi, R.P.; Neudeck, P.G.; Fazi, C. Analysis of the temperature dependent thermal conductivity of silicon carbide for high temperature applications. *J. Appl. Phys.* **2000**, *88*, 265–269. [\[CrossRef\]](#)
36. Burgemeister, E.A.; von Muench, W.; Pettenpaul, E. Thermal conductivity and electrical properties of 6H silicon carbide. *J. Appl. Phys.* **1979**, *50*, 5790–5794. [\[CrossRef\]](#)
37. Slack, G.A. Thermal conductivity of pure and impure silicon, silicon carbide, and diamond. *J. Appl. Phys.* **1964**, *35*, 3460–3466. [\[CrossRef\]](#)
38. Lienhard, J.H., IV; Lienhard, J.H., V. *A Heat Transfer Textbook*; Phlogiston Press: Cambridge, MA, USA, 2008.
39. Carslaw, H.S.; Jaeger, J.C. *Conduction of Heat in Solids*, 2nd ed.; Oxford University Press: New York, NY, USA, 1959.
40. Joyce, W.B. Thermal resistance of heat sinks with temperature-dependent conductivity. *Solid-State Electron.* **1975**, *18*, 321–322. [\[CrossRef\]](#)
41. Necati Özişik, M. *Boundary Value Problems of Heat Conduction*; Dover Publications: New York, NY, USA, 1989.
42. Poulton, K.; Knudsen, K.L.; Corcoran, J.J.; Want, K.-C.; Pierson, R.L.; Nubling, R.B.; Chang, M.-C.F. Thermal design and simulation of bipolar integrated circuits. *IEEE J. Solid-State Circuits* **1992**, *27*, 1379–1387. [\[CrossRef\]](#)
43. Rinaldi, N. Small-signal operation of semiconductor devices including self-heating, with application to thermal characterization and instability analysis. *IEEE Trans. Electron Devices* **2001**, *48*, 323–331. [\[CrossRef\]](#)
44. Codecasa, L.; d’Alessandro, V.; Magnani, A.; Rinaldi, N. Compact dynamic modeling for fast simulation of nonlinear heat conduction in Ultra-Thin Chip Stacking technology. *IEEE Trans. Components, Packag. Manuf. Technol.* **2014**, *4*, 1785–1795. [\[CrossRef\]](#)
45. Yeats, B. Inclusion of topside metal heat spreading in the determination of HBT temperatures by electrical and geometrical methods. In Proceedings of the Technical Digest of the IEEE GaAs Integrated Circuits (GaAs IC) Symposium, Monterey, CA, USA, 17–20 October 1999; pp. 59–62.
46. d’Alessandro, V.; Rinaldi, N. A critical review of thermal models for electro-thermal simulation. *Solid-State Electron.* **2002**, *46*, 487–496. [\[CrossRef\]](#)
47. Marsh, S.P. Direct extraction technique to derive the junction temperature of HBT’s under high self-heating bias conditions. *IEEE Trans. Electron Devices* **2000**, *47*, 288–291. [\[CrossRef\]](#)
48. Menozzi, R.; Barrett, J.; Ersland, P. A new method to extract HBT thermal resistance and its temperature and power dependence. *IEEE Trans. Device Materials Reliab.* **2005**, *5*, 595–601. [\[CrossRef\]](#)
49. Müller, M.; d’Alessandro, V.; Falk, S.; Weimer, C.; Jin, X.; Krattenmacher, M.; Kuthe, P.; Claus, M.; Schröter, M. Methods for extracting the temperature and power dependent thermal resistance for SiGe and III-V HBTs from DC measurements: A review and comparison across technologies. *IEEE Trans. Electron Devices* **2022**, *69*, 4064–4074. [\[CrossRef\]](#)
50. Bovolon, N.; Baureis, P.; Müller, J.-E.; Zwicknagl, P.; Schultheis, R.; Zanoni, E. A simple method for the thermal resistance measurement of AlGaAs/GaAs heterojunction bipolar transistors. *IEEE Trans. Electron Devices* **1998**, *45*, 1846–1848. [\[CrossRef\]](#)
51. Dawson, D.E.; Gupta, A.K.; Salib, M.L. CW measurements of HBT thermal resistance. *IEEE Trans. Electron Devices* **1992**, *39*, 2235–2239. [\[CrossRef\]](#)
52. Pfost, M.; Kubrak, V.; Brenner, P. A practical method to extract the thermal resistance for heterojunction bipolar transistors. In Proceedings of the IEEE conference on European Solid-State Device Research (ESSDERC), Estoril, Portugal, 16–18 September 2003; pp. 335–338.
53. Nenadović, N.; d’Alessandro, V.; La Spina, L.; Rinaldi, N.; Nanver, L.K. Restabilizing mechanisms after the onset of thermal instability in bipolar transistors. *IEEE Trans. Electron Devices* **2006**, *53*, 643–653. [\[CrossRef\]](#)
54. Zweidinger, D.T.; Fox, R.M.; Brodsky, J.S.; Jung, T.; Lee, S.-G. Thermal impedance extraction for bipolar transistors. *IEEE Trans. Electron Devices* **1996**, *43*, 342–346. [\[CrossRef\]](#)
55. Berkner, J. Extraction of Thermal Resistance and Its Temperature Dependence Using DC Methods. Presentation Held at HICUM Workshop, Dresden, Germany, 18–19 June 2007. Available online: https://www.see.et.tu-dresden.de/see/eb/forsch/Models/workshop0607/contr/Berkner_Infineon_HICUM_WS_2007_Dresden_070621s.pdf (accessed on 15 April 2022).
56. d’Alessandro, V. Experimental DC extraction of the thermal resistance of bipolar transistors taking into account the Early effect. *Solid-State Electron.* **2017**, *127*, 5–12. [\[CrossRef\]](#)
57. COMSOL Multiphysics User’s Guide, Release 5.2A, 2016. Available online: <https://www.comsol.it/> (accessed on 1 October 2020).
58. VBIC—Vertical Bipolar Intercompany Model, Release 1.2.1. Available online: <https://designers-guide.org/vbic/> (accessed on 15 April 2022).
59. van der Toorn, R.; Paasschens, J.C.J.; Kloosterman, W.J. *The Mextram Bipolar Transistor Model—Level 504.7*, Mextram Definition Document, March 2008. Available online: https://www.nxp.com/wcm_documents/models/bipolar-models/mextram/mextramdefinition_504.7.pdf (accessed on 15 April 2022).

60. AgilentHBT Model (Agilent Heterojunction Bipolar Transistor Model). Available online: <https://edadocs.software.keysight.com/pages/viewpage.action?pageId=6262855> (accessed on 15 April 2022).
61. Schröter, M.; Chakravorty, A. *Compact Hierarchical Bipolar Transistor Modeling with HICUM*; World Scientific Publishing: Singapore, 2010.
62. Schröter, M.; Pawlak, A. *HICUM/L2—A Geometry Scalable Physics-Based Compact Bipolar Transistor Model*, Documentation of Model Version 2.4.0, March 2017. Available online: https://www.iee.et.tu-dresden.de/iee/eb/forsch/Hicum_PD/Hicum23/hicum_L2V2p4p0_manual.pdf (accessed on 15 April 2022).
63. PathWave Advanced Design System (ADS) 2022. Available online: <https://www.keysight.com/zz/en/lib/resources/software-releases/pathwave-advanced-design-system-ads-2022.html> (accessed on 15 April 2022).
64. d'Alessandro, V.; D'Esposito, R.; Metzger, A.G.; Kwok, K.H.; Aufinger, K.; Zimmer, T.; Rinaldi, N. Analysis of electrothermal impact-ionization effects in bipolar cascode amplifiers. *IEEE Trans. Electron Devices* **2018**, *65*, 431–439. [CrossRef]
65. Codecasa, L.; d'Alessandro, V.; Magnani, A.; Irace, A. Circuit-based electrothermal simulation of power devices by an ultrafast nonlinear MOR approach. *IEEE Trans. Power Electron.* **2016**, *31*, 5906–5916. [CrossRef]